Quaternary International 758 (2026) 110114

Contents lists available at ScienceDirect

Quaternary International

journal homepage: www.elsevier.com/locate/quaint

Environmental change in SW Portugal during the last 3900 years BP: an Ostracoda assessment

Maria João Fernandes Martins [a,*], Maria Cristina Cabral [b,c], Vitor Hugo Magalhães [c,d], Teresa Drago [c,e], Francisco Fatela [b,c], Anabela Oliveira [c,f]

[a] ICArEHB - Interdisciplinary Center for Archaeology and the Evolution of Human Behaviour, Universidade do Algarve, Campus Universitário de Gambelas, Edifício A5.3, 8005-139, Faro, Portugal
[b] Departamento de Ciências da Terra e Energia, Faculdade de Ciências, Universidade de Lisboa, Campo Grande, C6, 1749-016, Lisboa, Portugal
[c] Instituto Dom Luiz (IDL), Faculdade de Ciências, Universidade de Lisboa, Campo Grande, C1, 1749-016, Lisboa, Portugal
[d] Instituto Português do Mar e da Atmosfera (IPMA), Marine Geology and Georesources Division, Rua C ao Aeroporto, 1749-077, Lisboa, Portugal
[e] Instituto Português do Mar e da Atmosfera (IPMA), IPMA station Tavira, Vale Caranguejo, Tavira, 8800-737, Portugal
[f] Instituto Hidrográfico, Rua das Trinas, 49, 1249-093, Lisboa, Portugal

ARTICLE INFO

Keywords:
Paleoenvironmental reconstruction
Algarve continental shelf
Holocene
Ostracods

ABSTRACT

Ostracod, geochemical, mineralogical, and sedimentological proxies from a sediment core collected off Sagres (southwestern Portugal) were used to reconstruct Holocene environmental and hydrodynamic changes.

Reduced variability of geochemical elements between ~4000 and ~1290 calibrated years before present suggests relatively stable conditions, regularly disturbed by higher-energy events. At ~1290 cal yrs BP, a transition from arid to wetter conditions is suggested based on enhanced terrestrial/detrital input after this time. Ostracod assemblages further captured fine-scale hydrodynamic variability, offering greater sensitivity to oceanographic changes.

Our results support a broader pattern of middle-to-late Holocene drying conditions in southern Iberia, followed by a shift to wetter conditions during periods of negative North Atlantic Oscillation (NAO) index. Our study provides new data on offshore ostracods from the western Algarve, underscoring their value for high-resolution paleoenvironmental reconstructions.

1. Introduction

The Iberian Peninsula occupies a unique climatic position in the Northern Hemisphere (e.g., Fiúza et al., 1982), with the mid-latitude North Atlantic system interacting with the subtropical climatic system of northern Africa (e.g., Pérez-Díaz et al., 2024). The combination of a dynamic climate and complex topography defines the Iberian Peninsula as an exceptional region for studying how contrasting biogeographical regions responded to past climatic variations (Pérez-Díaz et al., 2024). The study of past environmental and climatic fluctuations, such as transitions from warm periods and subsequent ecological recovery, is key to understanding today's climate change. Such transitions are well-known in the Holocene (e.g., Mayewski et al., 2004; Trouet et al., 2009).

However, general models are unable to account for the distinct sensitivities of each biogeographical region to climate change (Moreno et al., 2008; Pérez-Díaz et al., 2024). The paleoenvironmental data needed to improve models at a regional level are limited since many areas remain insufficiently studied (Moreno et al., 2008; Benito et al., 2015; Pérez-Díaz et al., 2024); this is particularly crucial since historical and current local-to-regional extreme events are increasingly recognised (e.g., Benito et al., 2015; Li et al., 2019; Báez et al., 2021). On the other hand, reliance on instrumental data is inadequate given the too-short time scale of such datasets, which exclude decadal-to-centennial external climate forcings (Abrantes et al., 2017; Santos et al., 2024). Thus, expanding paleoclimatic archives across biogeographical regions in Iberia is critical for improving local-to-regional climate models and future climate predictions.

A gap area is the southernmost tip of the Iberian Peninsula, Cape São Vicente (C.S. Vicente) in Portugal. The oceanographic regime in Portugal is dominantly governed by the North Atlantic Oscillation (NAO), an atmospheric pressure gradient between the Azores High (AH)

* Corresponding author.
E-mail address: mjfmartins@ualg.pt (M.J.F. Martins).

https://doi.org/10.1016/j.quaint.2025.110114
Received 6 August 2025; Received in revised form 7 November 2025; Accepted 31 December 2025
Available online 10 January 2026

and the Icelandic Low that drives seasonal wind patterns and precipitation (Fiúza et al., 1982; Trigo et al., 2004). Strong N-NE winds promote coastal upwelling along Portugal's Atlantic W coast from March to September (Fiúza et al., 1982), driven by the northward displacement of the AH and the weakening of the Icelandic Low (de Oliveira Júnior et al., 2024). In the Algarve region, however, maximum upwelling occurs around C.S. Vicente, with the southern coast's orientation limiting strong upwelling conditions to the east (Fiúza et al., 1982). In autumn, the southward shift of the AH brings moisture-rich westerlies to the western Iberian Peninsula (Trigo et al., 2004). Conversely, relaxation of upwelling-favourable winds favours a warm water counter-current that flows easterly or south-easterly, lacking clear seasonality (Garel et al., 2016). These factors make C.S. Vicente's oceanographic and climatic conditions uniquely distinct from those of the Atlantic Portuguese W coast and the eastern Algarve coast.

Under current climate projections, the expansion of the AH is expected to influence the position of the NAO relative to the Iberian Peninsula, leading to a decrease in precipitation in the region (e.g., Santos et al., 2024). Likewise, an increase in mean annual temperature is projected (e.g., Andrade et al., 2021). Considering these climate change predictions, combined with the human pressure of a tourism-driven economy in the Algarve, it is crucial to anticipate future climatic impacts.

To address this knowledge gap, we present paleoenvironmental data from a marine core collected off C.S. Vicente. We combine mineralogical, sedimentological, geochemical, and ostracod data to reconstruct Holocene environmental conditions. Ostracods – small aquatic crustaceans sensitive to temperature, salinity, sediment texture, and nutrient levels – are well-established paleoenvironmental proxies (e.g., Mazzini et al., 2021). Despite the potential, Holocene ostracod studies in Algarve remain limited to surface samples from the continental shelf and sediment cores from coastal lagoons and estuaries (e.g., Hindson et al., 1999; Luz, 2011; Cabral and Loureiro, 2013; Trog et al., 2013; Barata, 2021). Therefore, our research will equally contribute to a better understanding of the Ostracoda Holocene fauna on the Algarve continental shelf.

We compare our findings with published paleoenvironmental archives from the Algarve to gain a better understanding of past environmental variability in the C. S. Vicente region. We highlight the applicability of ostracods as sensitive paleoenvironmental proxies, confirming that *in situ* fossil assemblages can provide greater accuracy and higher-resolution insights into oceanographic changes than sedimentological records only (Camacho et al., 2017).

2. Regional settings

2.1. Regional geographic settings

Portugal is situated at the confluence of the Eurasian (Iberia subplate) and the African lithospheric plates (Mestdagh et al., 2019). The southern Portuguese continental shelf is narrow, reaching ~17–20 km at C. S. Vicente (e.g., Feist et al., 2025), with the continental shelf break occurring at about 110–150 m water depth (e.g., Feist et al., 2023). The Algarve basin comprises deposits of Mesozoic and Cenozoic age, overlaying a Palaeozoic basement (e.g., Feist et al., 2025); the littoral coast around Sagres is dominated by limestones, silts, marls and beach rock dated from the Jurassic to Miocene, with the occurrence also of sands and gravels dated to the Plio-Pleistocene (e.g., Chester, 2012). In the study area, watercourses and corresponding watersheds are small, providing limited runoff sedimentary detritus (Lobo et al., 2004; Feist et al., 2025). Coastal and shelf deposits input is predominantly the result of coastal cliff erosion (Dias et al., 2000), with the predominant southwest waves responsible for the eastward longshore current and sediment transport to the east (Boski et al., 2002). However, coastal counter-currents also affect the transport and deposition of inner-shelf sediments (Garel et al., 2016). Waves and storm-induced currents that transport sediment from other sections of the continental shelf are also of particular importance (Feist et al., 2025). Storm conditions are common on the Algarve coast, with strong seasonality associated with atmospheric systems (Oliveira et al., 2018).

2.2. Regional climatic settings

Portugal is located in the northern section of the climatic subtropical high-pressure belt of the Northern Hemisphere, with the region's climate and wind regime strongly dominated by the seasonal migration of the NAO (Fiúza et al., 1982; Trigo et al., 2004). From April to October, the AH displaces north, accompanied by the weakening of the Icelandic Low. This results in strong northerly winds (westerlies) favouring strong wind-driven upwelling currents along the Portuguese West coast (Relvas and Barton, 2002). In the southern coast, the C. S. Vicente area shows the most intense upwelling conditions; the southern coast's orientation limits strong upwelling conditions easterly (Fiúza et al., 1982). In autumn, the AH shifts southward (Fiúza et al., 1982), affecting the strength and direction of westerly, moisture-rich winds that reach Iberia (Trigo et al., 2004).

However, the relaxation of upwelling-favourable winds and the onset of the easterlies favour the circulation of a coastal, warm water tongue flowing westward from the Bay of Cádiz and curving up the western coast (Lobo et al., 2004; Garel et al., 2016). Consequently, the combination of these superficial oceanic currents leads to the formation of a cyclonic cell in the western section of the Algarve (with a second cell located in the eastern section; Mestdagh et al., 2019).

The current system, the superficial North Atlantic Superficial Water (NASW) dominantly flowing eastward into the Mediterranean, countered by the easterlies coastal circulation, is thus modelled by the prevailing wind (i.e., easterlies vs. westerlies) (Fiúza et al., 1982). The Algarve coast is under moderate wave activity (significant wave height off Faro: 0.92 m; Lobo et al., 2004), with two main wave regimes: 71 % of occurrences with a W-SW direction and 23 % SE-NW (Costa et al., 2001). Storm wave height increases to >3 m (Lobo et al., 2004). However, wave activity is minor at the water depth where our core was collected (85 m), since the storm wave base is ~30–35 m (Hernández-Molina et al., 2000). Furthermore, the study location is partly sheltered from W-SW waves by the C.S. Vicente (e.g., Feist et al., 2023).

In the northern margin of the Gulf of Cádiz, beneath the NASW, the Eastern North Atlantic Central Waters (ENACW) flow dominantly eastward at depths of ~100–250 m, affecting the outer shelf and upper slope seabed (Mestdagh et al., 2019). Below 400 m, poleward-flowing current carries warmer, more saline waters of Mediterranean (MOW) and subtropical origin (Moal-Darrigade et al., 2022). The MOW exits the Strait of Gibraltar moving north-westward along the Iberian margin, splitting into two cores shaped by the continental slope's morphology (Moal-Darrigade et al., 2022). Although it flows deeper than our study site, the MOW plays an important role in shaping intermediate water masses, indirectly influencing nutrient transport and slope current dynamics near C.S. Vicente (Sánchez-Leal et al., 2017).

The NAO index represents differences in atmospheric pressure between the Icelandic Low and the AH (Olsen et al., 2012). During the Holocene, a primarily negative NAO index was generally linked to increased precipitation in southern Iberia (e.g., Mendes et al., 2020). Conversely, drier and colder winters have been linked to positive NAO conditions in the region (Trigo et al., 2004; Mendes et al., 2020). Nevertheless, other atmospheric modes impact the North Atlantic climate, namely the east Atlantic (EA) and Scandinavia (SCAND) modes (Abrantes et al., 2017; Moreno et al., 2019), affecting precipitation variability at short scales in Iberia (Benito et al., 2015; Abrantes et al., 2017). Current climate change is influencing extreme short-term climatic oscillations, such as the NAO, leading to droughts, floods, or temperature extremes that affect ecosystems and ultimately resource management (e.g., Báez et al., 2021).

2.3. Previous ostracod studies

Previous seabed superficial samples collected at the location of our study site (Cabral et al., 2011; Luz et al., 2012; Cabral and Loureiro, 2013) identified distinct ostracod assemblages compared to seabed superficial samples collected eastward (from Lagos to V.R.S. António; Fig. 1) (Cabral et al., 2011; Luz et al., 2012; Cabral and Loureiro, 2013; Barata, 2021). The seabed superficial samples at our study site exhibited higher species richness associated with higher organic matter (productivity) content. This is likely an effect of increased coastal upwelling conditions at this location (Luz et al., 2012). The dominance of juveniles at distinct development stages over adults, i.e., the preferential transport of juveniles, indicates an overall low intensity of the hydrodynamic conditions.

2.4. Human occupation

Southwestern Algarve has a long history of human occupation (e.g., Bicho, 2009), with signs of human activities in marine and estuarine records dating back to ca. 5000 years (Fletcher et al., 2007; Delgado et al., 2012), with the economy primarily based on agriculture and pastoralism (Straus et al., 1992). Since the Iron Age (1200–550 BC; 3150–2500 cal yrs BP (calibrated years before present – 1950)), settlements intensified in coastal areas, such as Lagos, as indicated by the existing archaeological record (Chester, 2012).

Mining activities increased in southern Portugal in the second millennium BC, impacting settlement patterns, with fortified settlements appearing near mining resources or mineral transportation routes, such as along the Guadiana River, a natural southern border between the current territories of Portugal and Spain and connected to the Iberian Pyrite Belt (Cardoso, 2002). Mining activities reached their peak during the Roman Period (−200–500 CE; 1450–2150 cal yrs BP), evidenced by high Pb concentrations in this timeframe (Delgado et al., 2012; Mil-Homens et al., 2016, 2017), only reaching similar values following the 19th century Industrial Revolution (Mil-Homens et al., 2016).

However, human activities, such as deforestation, became a predominant landscape driver after the Medieval Islamic Period (700 CE–1300 CE; 1250–650 cal BP; Chester, 2012 and references therein). In the last ~1000 years, anthropogenic landscape change further increased, reflected in increased sedimentation rate in transition environments (e.g., former coastal estuaries in the Algarve; Schneider et al., 2010) and observed in the vegetation paleorecord (e.g., increasing values of open land communities; Schneider et al., 2016).

Today, the Algarve coastal area is heavily populated, with tourism a key economic driver (Omira et al., 2011), with high anthropogenic pressure in coastal environments (e.g., Chester, 2012). However, studies on long-term human impact are limited primarily to the east of Faro (e.g., Delgado et al., 2012; Mil-Homens et al., 2016, 2017).

3. Materials and methods

3.1. Coring and sampling

A sediment core 144 cm long (from here on referenced as POP14) was retrieved in 2008 in the Algarve continental shelf (36° 58′ 25.82″ N | 8° 52’ 3.83” W; Fig. 1) using a gravity corer at approximately 85 m water depth, in the framework of project POPEI (PDCT/MAR/55618/2004). The study site is situated at a lower bathymetry compared to the adjacent area (Fig. 1). The core was described based on changes in lithology, colour, boundaries and internal structure by visual inspection. The core was split horizontally and stored at 4 °C. Half of the core was archived and logged for non-destructive analysis, and the other half was subsampled at 1 cm intervals for multi-proxy analysis (each subsample ~5 cm^3 of wet sediment).

3.2. Chronology

The chronology of POP14 was constructed based on mass spectrometry (AMS) radiocarbon dating, a^{210}Pb profile, and a^{226}Ra profile. Six levels were determined for each isotope at the University of Bordeaux I (raw isotope data provided in Supplementary Table S1). Sample density g/cm^3 was obtained by sampling 3 cm^3 of sediment with the aid of a cut-off syringe. The 14C AMS dates were produced at Beta Analytic Inc., USA (Table 1). The age-depth model was produced in *R* v. 4.4.1 (R Core Team, 2022) and *RStudio* v. 2022.09.1 + 394 (RStudio Team, 2024) on a x86_64-w64-mingw32/x64 platform using *rplum* v. 1.0.0 (Aquino-López et al., 2018), following https://cran.r-project.org/

Table 1
POP14 AMS radiocarbon data. Calibrated radiocarbon dates provide 95 % probability minimum and maximum calibrated BP ages with *rplum* and *rbacon*.

Laboratory code	Depth (cm)	Material	Conventional radiocarbon age BP	$\delta^{13}C$ (‰)	Calibrated radiocarbon ages (95 % probability) BP (BCE/CE)
705052	34–35	Benthic foraminifera	1510 ± 30	−0.6	811–1152 (798–1139)
705053	98–99	Benthic foraminifera	3270 ± 30	−1.8	2459–3055 (509–1106)
278215	138	Gastropod shell	3930 ± 40	−2.8	3384–3949 (1434–1999)

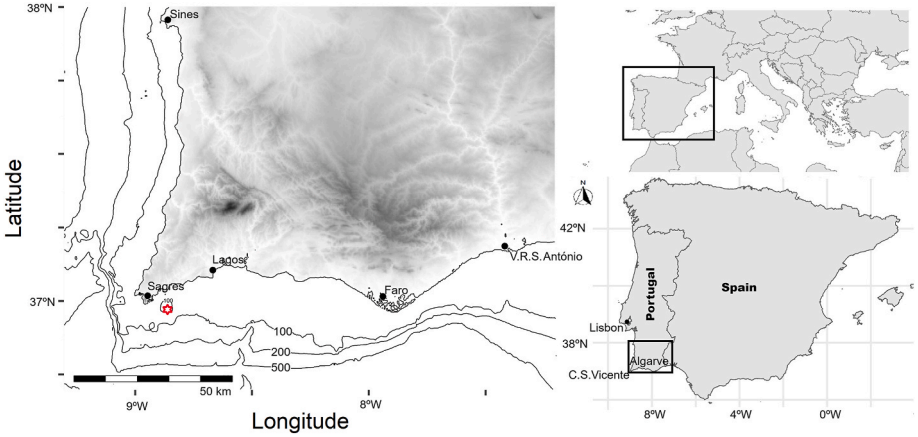

Fig. 1. Site location of sediment core POP14 (red star) and bathymetric map of southern Portugal. Black dots indicate the main cities. (For interpretation of the references to colour in this figure legend, the reader is referred to the Web version of this article.)

web/packages/rplum/vignettes/rplum.html (accessed May 2025). The mean supported ^{210}Pb was estimated using the ^{266}Ra data. ^{14}C dates were integrated by automatically calling *rbacon* v. 3.5.2 (Blaauw and Christen, 2011). The Marine20 calibration curve was used to correct the radiocarbon ages (Heaton et al., 2020), with the marine reservoir effect ΔR and its error retrieved following Soares and Valério (2024). This Bayesian approach uses Markov Chain Monte Carlo iterations (4000 iterations × 3 chains) to estimate age probability and sedimentation rates. The mean probability distribution was used for the sample's age estimation in calendar years before the present (cal yrs BP - 1950), with the 95 % CI shown between brackets at specific depths.

3.3. Mineralogy and sedimentology

Sedimentological analyses were conducted at 5 cm intervals at IPMA-Tavira, with a total of 28 samples analysed. The grain size was obtained using the Malvern Mastersizer 2000. Carbonate content analyses followed Scheibler's volumetric method with an Eijkelkamp calcimeter (Tatzber et al., 2007). The content of organic matter (OM) was determined using the loss-on-ignition (LOI) method: 200 mg of bulk sediment samples were placed in a muffle furnace at 450 °C for ca. 2 h (following Craft et al., 1991).

For the bulk mineralogical composition data, samples were dried at 40 °C and milled for X-ray diffraction (XRD) analyses at the Hydrographic Institute, performed on an X'Pert PANalytical diffractometer with CuKα radiation. Scans were run between 4° and 60° 2θ, in non-oriented powder mounts (samples). The peak areas of the specific reflections were calculated and weighted with empirically estimated factors for semi-quantification of the main minerals (Martins et al., 2007). The following minerals were identified: Aragonite, Calcite, Cal_{Mg}, Feldspar, Illite, Kaolinite, Opal, Plagioclase, Pyrite, and Quartz (Supplementary Table S1). Infrequent traces of Anhydrite, Chlorite, Dolomite, and Siderophyllite were identified; these minerals were excluded from posterior analysis. In total, 28 samples were analysed following the same sampling scheme as the sedimentological analysis.

3.4. Geochemistry

Geochemical elements quantification was done every 1 cm at MARUM - University of Bremen, with an AVAATECH X-Rays Fluorescence (XRF) Core Scanner, scanned at 10 kV with a 0.2 mA current and no filter, and a 20 s live time to measure Al, Si, S, K, Ca, Ti, Mn and Fe contents. Cores were scanned at 30 kV with a 1.0 mA current and a 20 s live time, with a Pd filter for Br, Rb, Sr, Zr and Pb (while Pb showed low count values, trends are indicative of consistent values). 137 depth measurements were analysed, with data gaps occurring on too coarse-grained or too uneven sediment surfaces for correct sensor measurements (Supplementary Table S1).

3.5. Ostracoda

The ostracods were analysed for 14 samples, collected at 10 cm intervals. Samples were wet sieved using a 63 μm mesh, deflocculated (with sodium hexametaphosphate, $Na_6O_{18}P_6$), dried (at a maximum of 40 °C), and sieved again in a 1ϕ logarithmic scale interval (63 μm, 125 μm, 250 μm, 500 μm, 1000 μm and 2000 μm). Using fractions 125 μm and above, all ostracod individuals in each sample were picked under a stereomicroscope and counted, with one valve = one carapace = one individual (hereafter referred to as the **species dataset**). The individuals were identified to the species level where possible, primarily following Bonaduce et al. (1976), Athersuch et al. (1989), Luz (2011), Cabral and Loureiro (2013), and Barata (2021).

Ostracod densities were standardised to the number of individuals per gram of bulk dry sediment before statistical analysis (number of specimens/g). Relative abundances were converted to percentages, and taxa were categorised into four groups: dominant, common, sparse and rare (roughly following Avolio et al., 2019). Dominants are autochthonous species with high abundance (i.e., >10 % relative frequency and represented by adult and juvenile forms at distinct stages of development). The taxa with a relative abundance >5 % (but <10 %) in at least one sample were defined as common (considered widespread and locally abundant relative to other species in the assemblage, except dominant species). Sparse species are present in >50 % of samples at low frequencies (<5 %). Taxa identified to the species level that did not meet these criteria were classified as rare. Unlike Avolio et al.'s (2019) definition, in our core, rare species can be geographically widespread.

Identification at the species level in several genera, such as *Hemicytherura* and *Semicytherura,* is only possible in adults. Moreover, a high proportion of juvenile ostracods are unidentifiable. To account for these limitations, we also analyse the ostracod data at the genus taxonomic level. The genus-level data is referred to as the **genera dataset**, providing additional insights into broader community trends.

Selected specimens were photographed using a scanning electron microscope (SEM) at the Faculty of Sciences, University of Lisbon, for documentation and identification purposes.

3.6. Statistical analysis

Statistical analyses were performed using *R* v. 4.4.1 (R Core Team, 2022) and *RStudio* v. 2022.09.1 + 394 (RStudio Team, 2024). Fig. 1 was produced with R packages *geodata* v. 0.6–2, *marmap* v. 1.0.10 (following https://www.moleculareecologist.com/2015/07/marmap/; accessed on March 2025), and *ggplot2* v. 3.5.1 (Wickham, 2016).

Sedimentary and mineralogical proxies are expressed as percentages, and a Principal Component Analysis (PCA) was conducted using the base R function *prcomp* (with options scale and centre = T); highly correlated elements were removed (Pearson correlation >0.75; Supplementary Table S1). Results for each geochemical element were expressed as counts per second and Ti normalised (Supplementary Table S1). Highly correlated elements were removed following a Spearman correlation test (Supplementary Table S1). The core first and last cm were excluded from the PCA analysis.

The absolute abundances (number of specimens/g) of common, dominant, rare, and sparse species were used to calculate species diversity (Shannon Index or H; Shannon, 1948) and evenness (Pielou's Evenness or J; Pielou, 1966). Common, dominant, and sparse species were used in a cluster analysis carried out with the Constrained Incremental Sum of Squares (CONISS) approach and the Bray-Curtis distance, using the broken-stick model to establish stratigraphically consecutive zones (e.g., Ejarque et al., 2016). Abundances were log10 (x+1) transformed prior to analysis to address distributional skewness (e.g., Ejarque et al., 2016). The ratio of intact-to-broken valves was used as an index of preservation. These analyses were conducted using the R package *vegan* v. 2.6–6.1 (Oksanen et al., 2025).

Stratigraphic diagrams of selected proxies were produced using *R* packages *rioja* v. 1.0–6 (Juggins, 2024), *riojaPlot* v. 0.1–24 (following https://nsj3.github.io/riojaPlot_gallery/riojaPlot_Gallery.html#1) and *ggplot2*.

4. Results

4.1. Chronology

The radiocarbon date nearest to the base of POP14 indicates that the core is approximately 4000 cal yrs BP (Table 1). Using the age model output from *rplum* and *rbacon* (Fig. 2), the mean modelled calibrated radiocarbon ages, with the 95 % confidence interval (CI) shown between brackets, are used at specific depths in the following sections.

4.2. Sedimentology, mineralogy and geochemistry

Core POP14 comprises fine sediments with well-preserved laminae,

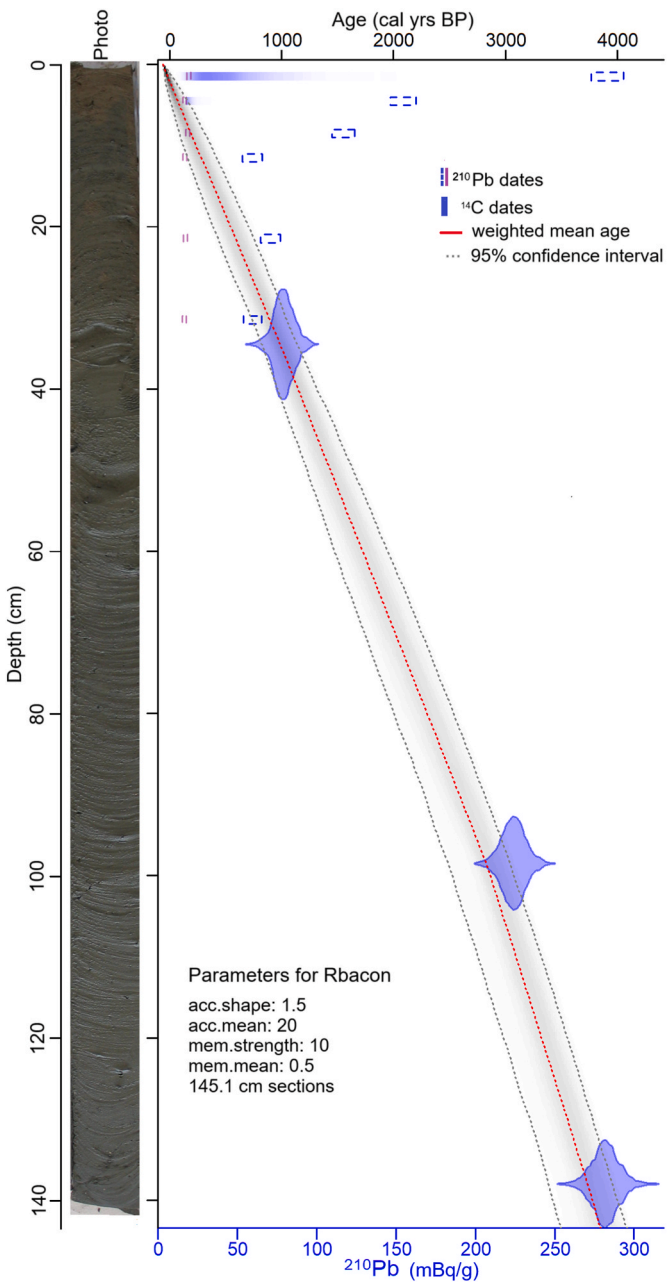

Fig. 2. Bayesian age-depth model for sediment core POP14 and core photograph. Variable ^{226}Ra was used to calculate supported ^{210}Pb in *rplum* program. The grey curve and shading represent the final, full-core Bayesian model integrating constraint ^{210}Pb and ^{14}C dates in *rbacon*.

particularly between ~115–55 cm and ~30–10 cm, indicating regular changes in sedimentation rates (Fig. 2). The sediment is darker in the lower section of the core (greenish-black 5GY 2/1; Munsell Colour, 1995), changing at 50 cm to a dark greenish-grey (5GY 4/1) and olive-grey colour (5Y 4/1) at the top 5 cm. Some bioturbation is visible in the first 20 cm (Fig. 2 photo).

The grain-size analysis shows a mean grain size of approximately 60 μm, increasing to about 70 μm between 80 cm and 30 cm depth (Fig. 3A). The predominant textural type is silt (range: ~45 %–60 %), followed by sand (range: ~28–47 %), with uniform clay content at ~10 % (Fig. 3A). The core is classified as muddy sand according to the Flemming classification (Flemming, 2000). The carbonate content is high (range: 34–47 %; Fig. 3A) and roughly follows the sand profile. Organic matter content (OM) is relatively stable (range: ~3–5 %; Fig. 3A). Calcite is the most abundant mineral (range: ~42–62 %), followed by quartz (range: ~9–16 %) (Fig. 3A). Accessory minerals include aragonite (<6 %), Cal_{Mg} (<12 %), feldspar (<12 %), illite (<10 %), kaolinite (<7 %), opal (<4 %), plagioclase (<6 %) and pyrite (<8 %) (Supplementary Table S1).

All textural elements are highly correlated, with sand percentage retained for the PCA analysis of the mineralogy and sedimentology matrix (Fig. 3B; Supplementary Table S1). The first principal component (PC1) explains over 22 % of the variance (Fig. 3B), clustering Cal_{Mg}, carbonate, feldspar, opal and sand content (positive PC1 values) in opposition to calcite, quartz, and kaolinite (negative PC1 values). PC2 explains over 15 % of the variance, clustering plagioclase and OM in opposition to pyrite (Fig. 3B).

The mineralogy and sedimentology PC1 can be divided into three main zones (MSZ-I to III), based on maximum and minimum values (Fig. 3A). In the lower core section, PC1 values are generally negative, reaching their lowest value at a depth of 80 cm (2296 (1990–2541) cal yrs BP). The fine-grain fraction dominates, intercalated by periods of slightly higher sand content. Calcite concentrations crudely track variations in mean grain size, while the tracking of carbonates and quartz concentrations relative to the mean grain size is less pronounced. From a depth of 80 cm–30 cm, PC1 values trend upward, reflecting the gradual increase in mean grain size. Between ~60 cm and 30 cm of depth, sand and silt occur in similar proportions (Fig. 3A) with calcite content remaining stable during this interval, unlike quartz and pyrite. The phyllosilicate content (illite, kaolinite) reached its highest concentrations just before the period of relative stability in mean grain size. In contrast, feldspar and plagioclase content rise more pronouncedly after ~45 cm. At ~30 cm depth (853 (684–1008) cal yrs BP), PC1 reaches its highest value (Fig. 3A), followed by a decrease in sand and carbonate content after this point, with a slight rise in organic matter, reflected in increasingly negative PC1 values (Fig. 3A).

In the geochemical matrix, PC1 explains over 35 % of the variance (Fig. 3C), and it clusters Al and K (negative values) against Ca, Fe, Mn, Rb, S, and Zr (positive values). (Element Sr, which was highly correlated to Ca and Zr, was removed from the geochemical PCA analysis; see Supplementary Table S1.) PC2 explains more than 21 % of the variance and clusters Br, Ca, Si, and Pb with negative values.

PC1 Geo shows two zones (GZ-I to II): the top ~45 cm has negative PC1 values; the lower section fluctuates around one (with exceptions, such as ~125 cm of depth; Fig. 3A), characterised by cyclic variation in weathering elements (SI, Al, Fe) relative to biogenic elements (Ca, Sr). The transition to PC1 negative values is precluded by a peak in S, Mn, and Fe concentrations, with PC1 Geo reaching its highest values at a depth of 45–50 cm. At ~45 cm (1292 (1092–1494) cal yrs BP), the transition to PC1 negative values marks increased terrestrial input proxies (Al, Si), and a decrease in Ca and Sr (biogenic proxies), Fe (linked to siliciclastic weathering), and S (a contributor to pyrite) above this depth (Fig. 3A).

Element Br, often used as a proxy for organic matter in marine settings (productivity; Val-Peón et al., 2021), shows a concentration peak at ~80 cm, paralleling decreased sand content (Fig. 3A). The same pattern is observed in the top ~20 cm of the core. Pb, used as an indicator of human activities (e.g., Mil-Homens et al., 2017; Mendes et al., 2020), also increases gradually from about 20 cm depth (549 (391–707) cal yrs BP) to the last analysed sample (5 cm; 91 (8–203) cal yrs BP), with notable peaks at ~70-65 cm and ~47 cm depths (1448 (1142–1552) cal yrs BP; Fig. 3A).

4.3. *Ostracoda:* ***species dataset***

A total of 87 species, assigned to 51 genera, were identified in the fraction ≥125 μm; the species list is provided as Appendix A, and the systematic species list is provided in Supplementary Table S2. The assemblages are primarily composed of juveniles (range: 65–84 %; Fig. 4A), with only a few articulated carapaces found. This suggests a

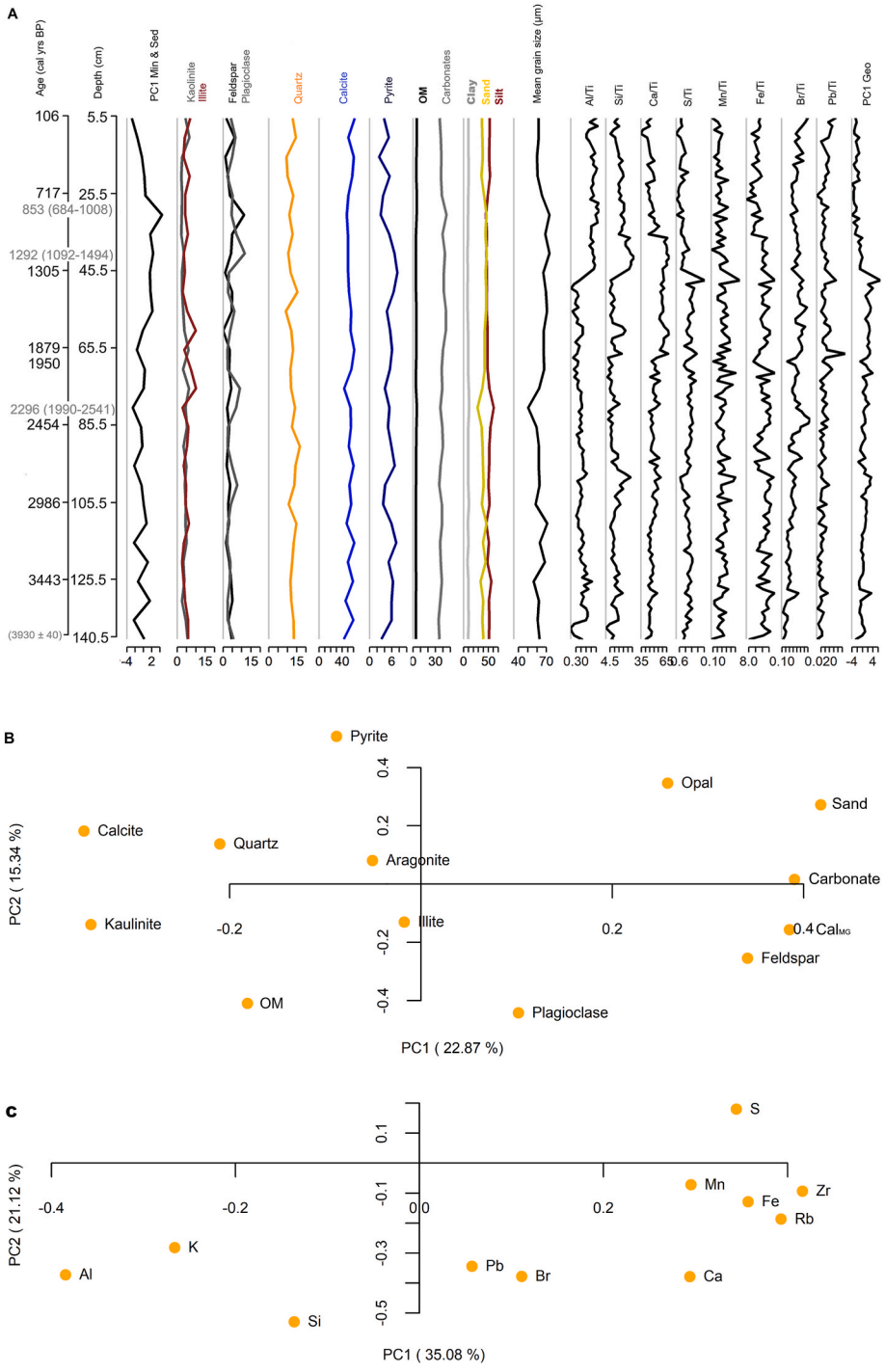

Fig. 3. POP14 selected mineralogical & sedimentological data (concentration as %), geochemical elements and PCA analysis. (A) The first column corresponds to the sample distribution according to the PCA first eigenvector for the mineralogical and sedimentology matrix. The last column corresponds to the PCA first eigenvector for the geochemical matrix. Mean modelled calibrated radiocarbon ages in black; at key zonation transitions, mean ages are presented with the 95 % CI in brackets, and the conventional ^{14}C age (BP) of the core base is displayed in grey; (B) PCA of the mineralogical and sedimentological content; (C) PCA of the geochemical elements content.

depositional location with low hydrodynamics that favour juvenile valve transport. The percentage of undetermined specimens or those identified only to the genus level varied between ~23 % (sample 25.5 cm) and ~13 % (115.5 cm).

The evenness index varied between 0.89 (sample 15.5 cm) and 0.78 (105.5 cm), indicating relatively uniform species abundances across samples (i.e., J range from 0 to 1, where 1 means all species have an equal number of values). The preservation index ranged from ~88 % (5.5 cm) to ~70 % (85.5 cm depth), with no clear trend across the core (Fig. 4A).

Nine species exhibited relative abundances ≥5 % in at least one sample (Fig. 4A), with the sublittoral species *Costa runcinata* the only dominant species (range: ~14–25 %; Fig. 4A; relative abundances are shown in Supplementary Table S2). The relative abundances of the 23 sparse species (i.e., species present in at least 8 of the 14 samples and with <5 % relative abundance) are shown in Fig. 4B.

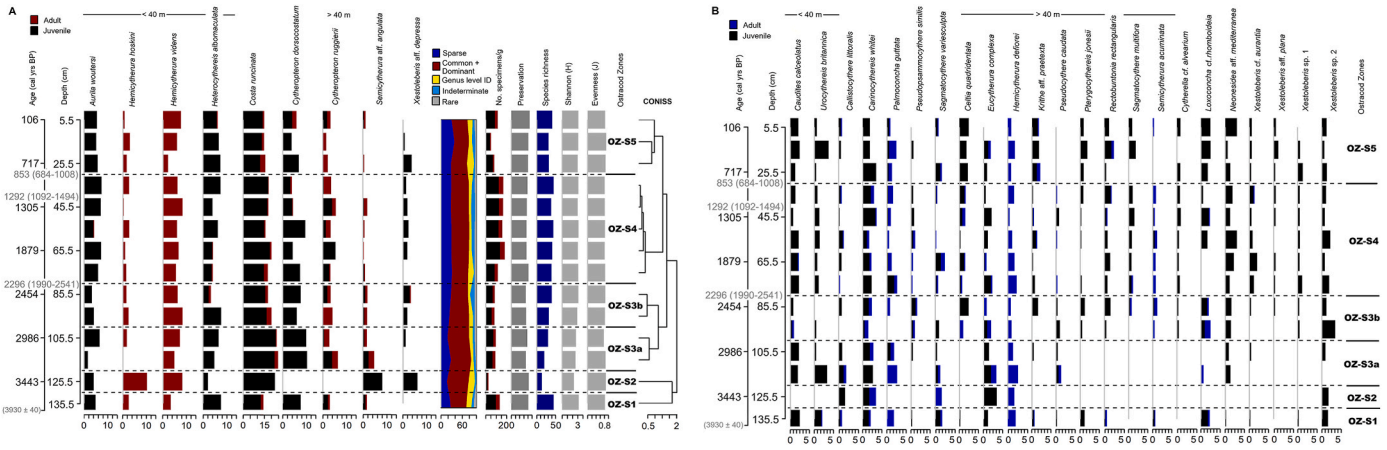

Fig. 4. POP14 Ostracod stratigraphic diagram for the **species dataset**. (A) Dominant and common species relative frequencies (i.e., >10 % and >5 % in one sample at least, respectively), the cumulative frequency of dominant, common, sparse, rare, undetermined or identified to the genus level, number of valves per sample (number of specimens per sample standardised to 1 g of dry sediment), preservation index (ratio of intact-to-broken valves), species richness (number of species), Shannon diversity index, Evenness, and dendrogram from the CONISS cluster analysis and ostracod zones **species dataset** – OZ-S. (B) Sparse species relative frequencies (i.e., present in >50 % of samples with a relative frequency <5 %). Mean modelled calibrated radiocarbon ages in black; at key zonation transitions, mean ages are presented with the 95 % CI in brackets, and the conventional ^{14}C age (BP) of the core base is displayed in grey.

Ostracod species were grouped based on water depth preferences: <40 m and >40 m (Fig. 4), roughly aligning with Algarve continental shelf zones (inner shelf: <40 m, median shelf: 40–90 m; following Lopes and Cunha, 2010). No information is given to species with broad depth preferences (such as *C. runcinata*, *Callistocythere littoralis*) or open species taxonomic assignment (such as *Loxoconcha* cf. *rhomboideia*, *Xestoleberis* sp. 1). Unknown water depth preferences occur in ~46 % of the rare species category. All the common species preferring water depth <40 m are phytal-associated (Fig. 4A), while this pattern does not hold for the sparse species group (i.e., *Urocythereis britannica* and *Caudites calceolatus* do not associate with aquatic vegetation) (Fig. 4B).

The cluster analysis (based on absolute abundances of common, dominant and sparse species) indicates that both five and six zones are acceptable (CONISS dendrogram, OZ-S1 to 5; Fig. 4A). To simplify, the ostracod zone **species dataset** 3 was split into OZ-S3a and OZ-S3b. Calibrated dates are the mean modelled calibrated radiocarbon ages, with the highest and lowest values used to define the 95 % CI for each zone between brackets.

- OZ-S1 (135–136 cm; 3662–3685 (3318–3904) cal yrs BP): Highest species richness and Shannon diversity index (45 species, H = 3.17; Fig. 4A).
- OZ-S2 (125–126 cm; 3432–3454 (3090–3660) cal yrs BP): Lowest species richness and Shannon diversity (13 species, H = 2.24). The lowest total valve counts (24 specimens/g); rare forms are almost absent. Marked by a near absence of species typical of >40 m depth (e.g., *Cytheropteron ruggierii*, *Pterygocythereis jonesii*, *Rectobuntonia rectangularis*) and non-phytal littoral species with a preference for depths <40 m (*Aurila woutersi*, *U. britannica*). This is reflected in the lower value of the cumulative relative frequency of sparse species (Fig. 4A).
- OZ-S3 (85–116 cm; 2439–3226 (2125–3455) cal yrs BP): Increasing species richness, with the gradual reappearance of species preferring >40 m depths, a pattern more intense in OZ-S3b.
- OZ-S4 (35–76 cm; 1004–2180 (837–2423) cal yrs BP): Highest total valve counts; overall, higher species richness relative to OZ-S3 (Fig. 4A).
- OZ-S5 (5–26 cm; 91–732 (8–895) cal yrs BP): Reduction in total valve counts, characterised by the absence/negligible occurrence of *Pseudocythere caudata* and *Semicytherura acuminata* compared to OZ-S4. Despite this, a slight increase in the proportion of sparse species relative to common + dominant species is observed (Fig. 4A).

4.4. *Ostracoda:* ***genera dataset***

Fifty-one genera were identified (Appendix A; Supplementary Table S2). Evenness values range from ~0.76 to ~0.89 (Fig. 5A), suggesting some uniformity in the absolute abundances of genera across samples. Fig. 5A and B shows the relative abundances of the five dominant and two common, and 18 sparse genera (following the same category rules defined for the species-level analysis), respectively.

The cluster analyses identified six zones (OZ-G1 to 6) based on the common, dominant and sparse genera (Fig. 5). Calibrated dates are the mean modelled calibrated radiocarbon ages, with the highest and lowest values used to define the 95 % CI for each zone between brackets.

- OZ-G1 (135–136 cm; 3662–3685 (3318–3904) cal yrs BP): Highest genera richness (34 genera).
- OZ-G2 (125–126 cm; 3432–3454 (3090–3660) cal yrs BP): Marked by the absence of several genera (e.g., *Cytheropteron*, *Celtia*), indicating changes in hydrodynamic conditions. The genus *Hemicytherura* dominated, contrasting with the dominance of *C. runcinata* at the species level. Lowest genera richness and Shannon diversity index (11 genera, H = 1.95).
- OZ-G3 (105–116 cm; 2975–3226 (2624–3455) cal yrs BP): Return of several genera and increased genera richness.
- OZ-G4 (55–96 cm; 1578–2755 (1349–2978) cal yrs BP): Genera richness approached OZ-G1 values.
- OZ-G5 (25–46 cm; 701–1319 (536–1523) cal yrs BP): The absence or differences in relative frequencies of specific genera (e.g., *Caudites*, *Carinocythereis*) distinguished this zone from OZ-G4.
- OZ-G6 (5–16 cm; 91–428 (8–587) cal yrs BP): The absence of *Pseudocythere,* in combination with differences in relative frequencies of specific sparse genera (e.g., *Carinocythereis, Caudites*), distinguishes this zone from OZ-G5. The highest Shannon index occurs at a depth of 5.5 cm (H = 2.87).

Ostracods from the 63–125 μm fraction were also analysed. As expected, most individuals in this fraction are juveniles (range: 76 %–96 %; data not shown). Moreover, analysing the data by combining all fractions is akin to that of the dataset species ≥125 μm presented in the article. Therefore, this data (and analysis) was not included in the present article.

A composite figure correlating the various studied proxies is provided in Fig. 6. Scanning electron microscope (SEM) images of the

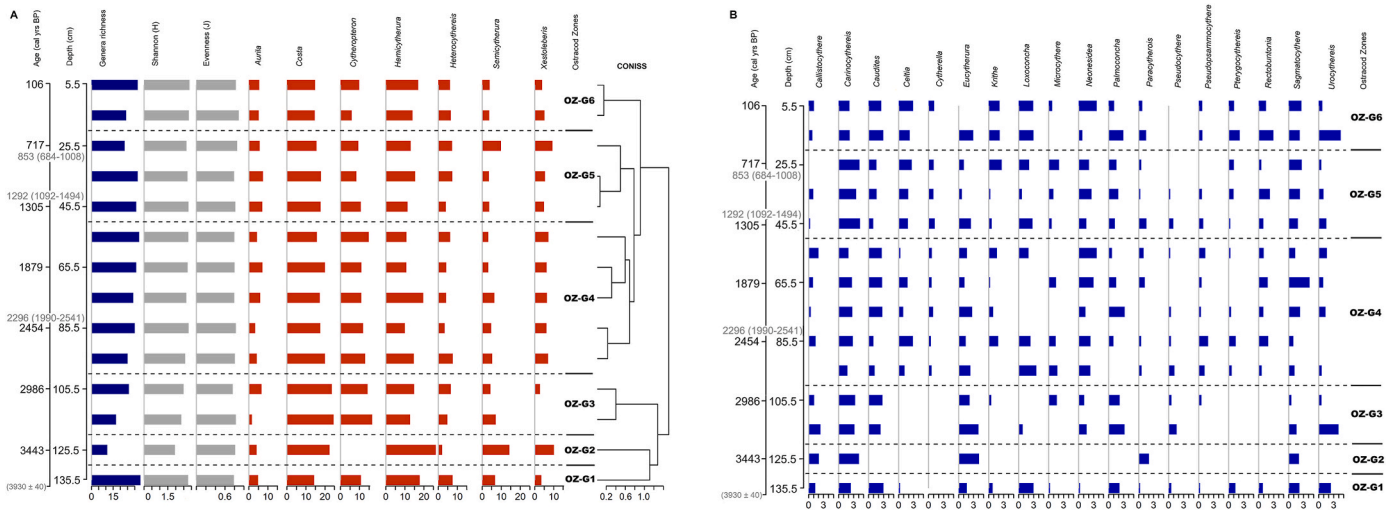

Fig. 5. POP14 Ostracod stratigraphic diagram for the **genera dataset**. (A) Genera richness (number of genera), Shannon diversity index, Evenness and relative frequencies of the dominant and common genera (i.e., >10 % and >5 % in one sample at least, respectively), and dendrogram from the CONISS cluster analysis and ostracod zones **genera dataset** – OZ-G. (B) Sparse species relative frequencies (i.e., present in >50 % of samples with a relative frequency <5 %). Mean modelled calibrated radiocarbon ages in black; at key zonation transitions, mean ages are presented with the 95 % CI in brackets, and the conventional ^{14}C age (BP) of the core base is displayed in grey.

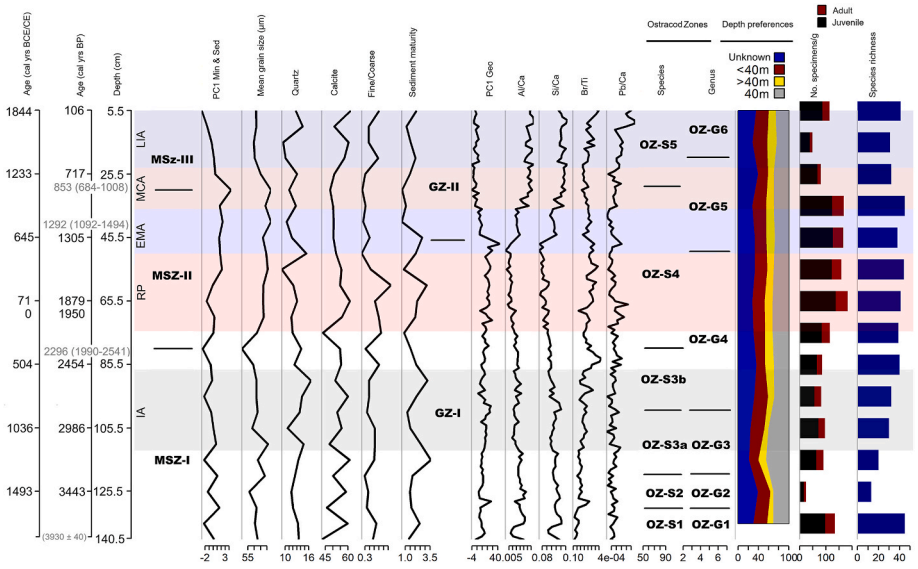

Fig. 6. POP14 composite diagram correlating key selected proxies. The first component of the mineralogy and sedimentology matrix PCA analysis (PC1 Min & Sed and respective zones MSZ-I to III), mean grain size, selected minerals (%), fine/coarse ((illite + kaolinite)/[quartz + feldspar + plagioclase]) and sediment maturity (quartz/[feldspar + plagioclase]); the first component of the geochemical matrix PCA analysis (PC1 Geo and respective zones GZ-I to II), selected geochronological elements and ratios; ostracod zones at the species- and genus-level according to the CONISS cluster analysis (OZ-S1 to 5 and OZ-G1 to 6, respectively), the cumulative relative frequency of species according to water depth preference, number of specimens per sample standardised to 1 g of dry sediment (no. specimens/g), and species richness (number of species). Mean modelled calibrated radiocarbon ages in black; at key zonation transitions, mean ages are presented with the 95 % CI in brackets, and the conventional ^{14}C age (BP) of the core base is displayed in grey. IA - Iron Age (date after Chester, 2012); RM - Roman Period; EMA - Early Middle Ages; MCA - Medieval Climate Anomaly; LIA - Little Ice Age (dates after Sánchez-López et al., 2016).

dominant, common and sparse species are provided in Figs. 7 and 8.

5. Discussion

5.1. Ostracoda assemblages

POP14 ostracod assemblages have overall high species richness. The near-absence of articulated valves (carapaces) and the low abundance of adults suggest that most species are transported, along with sediments, from surrounding areas. *Costa runcinata* is the only species represented by juveniles at distinct stages of development and adults, indicating a likely autochthonous population and the only dominant species in the record (relative frequency >10 %).

The predominance of juvenile forms and signs of valve transportation (i.e., valve erosion) combined with a high preservation index (Fig. 4A) supports the idea of an area with generally low hydrodynamics, where currents primarily transport juveniles from the surrounding areas. The assemblages contain species with varied depth preferences, reflecting no specific transport from any continental shelf zone (i.e., no preference for the littoral, inner, middle, or outer platform). However, the allochthonous common species are favourably represented by coastal, phytal forms such as *A. woutersi* or

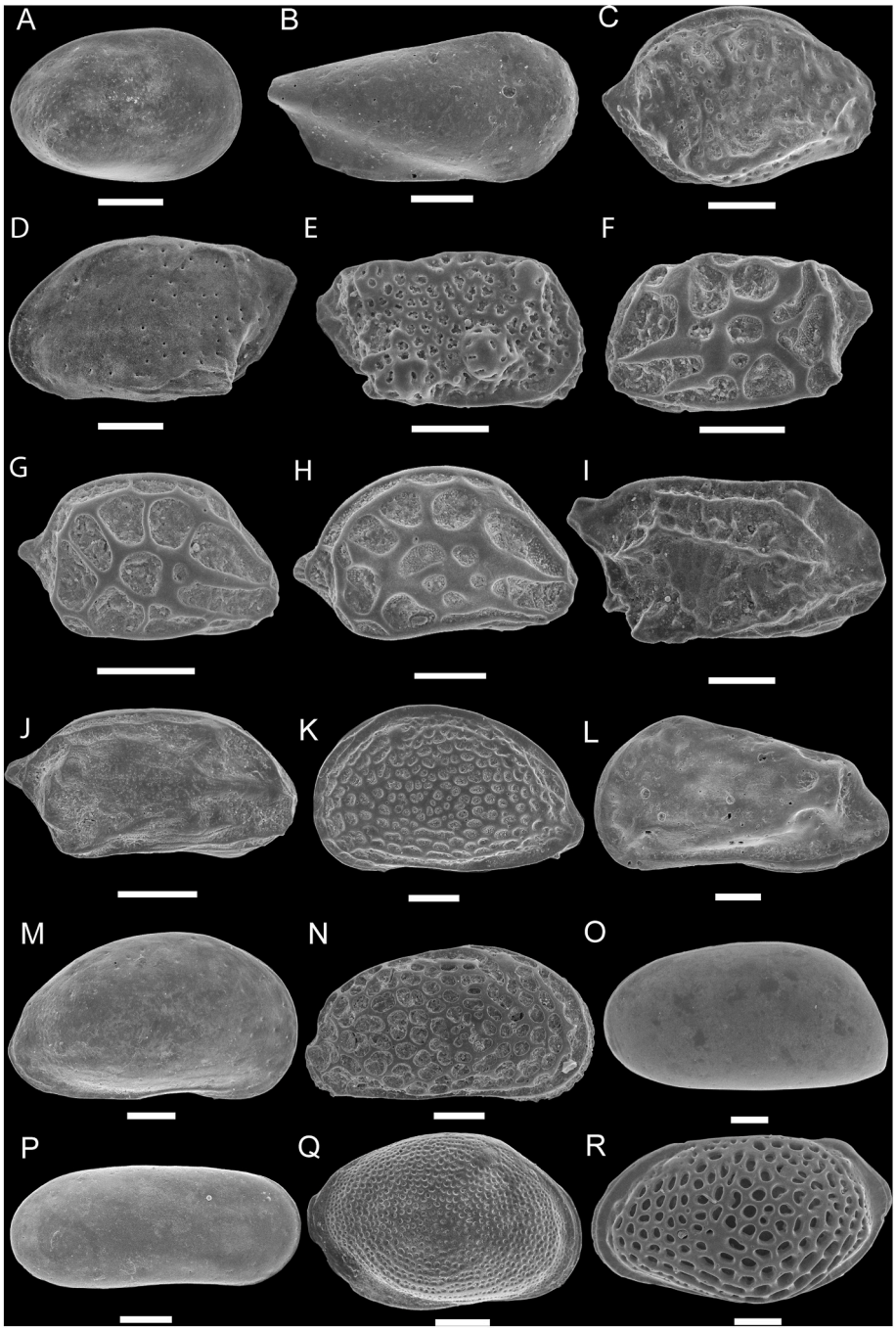

Fig. 7. POP14 common and sparse ostracod species. All species in lateral external view. A. *Cytherella* cf. *alvearium* Bonaduce et al., 1976, juvenile RV, sample 55.5 cm; B. *Pseudocythere caudata* Sars, 1886, RV, sample 35.5 cm; C. *Cytheropteron dorsocostatum* Whatley and Masson, 1980, juvenile RV, sample 135.5 cm; D. *Cytheropteron ruggierii* Pucci, 1955, LV, sample 75.5 cm; E. *Eucytherura cfi'omplexa* (Brady, 1866), RV, sample 75.5 cm; F. *Hemicytherura defiorei* Ruggieri, 1953, LV, sample 65.5 cm; G. *Hemicytherura hoskini* Horne, 1981, RV, sample 55.5 cm; H. *Hemicytherura videns* (G. W. Müller, 1894), RV, sample 65.5 cm; I. *Semicytherura acuminata* (G. W. Müller, 1894), RV, sample 35.5 cm; J. *Semicytherura* aff. *angulata* (Brady, 1868), RV, sample 125.5 cm. K. *Aurila woutersi* Horne, 1986, juvenile LV, sample 135.5 cm; L. *Caudites calceolatus* (O. G. Costa, 1853), juvenile LV, sample 45.5 cm; M. *Heterocythereis albomaculata* (Baird, 1838), juvenile RV, sample 135.5 cm; N. *Urocythereis britannica* Athersuch et al., 1989, juvenile RV, sample 115.5 cm; O. *Krithe* aff. *praetexta* (Sars, 1866), LV, sample 135.5 cm; P. *Pseudopsammocythere similis* (G. W. Müller, 1894), RV, 75.5 cm; H. *Loxoconcha* cf. *rhomboideia*, RV, sample 45.5 cm; R. *Palmoconcha guttata* (Norman, 1865), LV, sample 135.5 cm. LV – left valve; RV – right valve. Bar = 100 μm.

Heterocythereis albomaculata, whose presence likely reflects transport from productive nearshore habitats favoured under upwelling-influenced conditions in the study area from March to September (e.g., de Oliveira Júnior et al., 2024). Nevertheless, species with a preference for waters deeper than 40 m are present in the common, sparse and rare species category (Fig. 4).

On the other hand, the high species richness is also the result of the accumulation of typically Mediterranean species (e.g., *C. calceolatus, C. ruggierii* and *Pseudopsammocythere similis;* Bonaduce et al., 1976), as well as Atlantic species (e.g., *A. woutersi, Celtia quadridentata, Pontocythere elongata,* and *U. britannica;* Athersuch et al., 1989). This pattern serves as evidence of the importance of the dominant easterly flow of the NASW, and wind-driven upwelling during March to September (Fiúza et al., 1982; Relvas and Barton, 2002), together with the Mediterranean

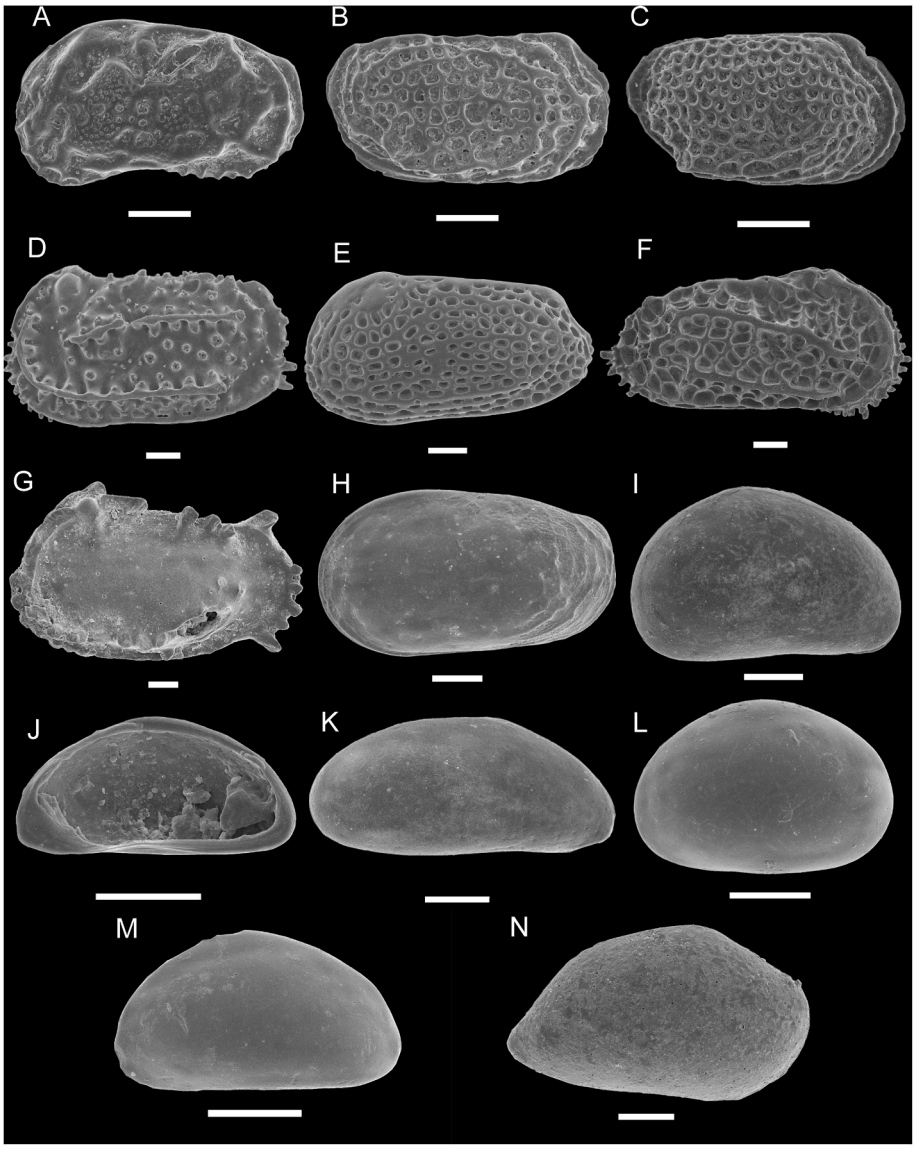

Fig. 8. POP14 dominant, common and sparse ostracod species. All species in lateral external view, except where indicated (IV – internal view). A. *Callistocythere littoralis* (Müller, 1894), LV, sample 135.5 cm; B. *Sagmatocythere multifora* (Norman, 1865), RV, sample 75.5 cm; C. *Sagmatocythere variesculpta* (Ruggieri, 1962), RV, sample 65.5 cm. D. *Carinocythereis whitei* (Baird, 1850), LV, sample 55.5. cm; E. *Celtia quadridentata* (Baird, 1850), LV, sample 35.5 cm; F. *Costa runcinata* (Baird, 1850), RV, sample 55.5 cm; G. *Pterygocythereis jonesii* (Baird, 1850), LV, sample 95.5 cm; H. *Rectobuntonia rectangularis* (Ruggieri, 1954), LV, sample 15.5 cm; I. *Xestoleberis* cf. *aurantia* (Baird, 1838), juvenile RV, sample 35.5 cm; J. *Xestoleberis* aff. *depressa* Sars, 1866, juvenile IVRV, sample 55.5 cm; K. *Xestoleberis* aff. *plana* G. W. Müller, 1894, juvenile RV, sample 85.5 cm; L. *Xestoleberis* sp. 1, juvenile LV, sample 25.5 cm; M. *Xestoleberis* sp. 2, juvenile LV, sample 75.5 cm; N. *Neonesidea* aff. *mediterranea* (Müller, 1894), juvenile RV, sample 5.5 cm. LV – left valve; RV – right valve. Bar = 100 μm.

counter-current along the Algarve coast (Fiúza et al., 1982; Garel et al., 2016). Moreover, the bathymetric location of the study site (lower than that of the adjacent areas) promotes the accumulation of valves. The evenness values above 0.75 suggest similar low frequencies among many taxa. These results align with the findings of Luz (2011) and Luz et al. (2012) from two seabed superficial samples collected in the same area as our study site.

Lastly, the rare identification of brackish-marine forms, such as *Basslerites teres, Loxoconcha elliptica, and S. tela,* as well as the single freshwater juvenile form putatively assigned to the genus *Cypris?,* suggests a limited influence from these environments. This pattern is not surprising, given the absence of major fluvial influence in this area of the Algarve coast (e.g., Lobo et al., 2004; Feist et al., 2023).

5.2. *Why does the species-level cluster analysis differ from the genus-level analysis?*

The CONISS cluster approach identified six ostracod zones in the **species dataset** and the genus-level analysis (**genera dataset**). However, differences are evident between datasets (Fig. 6), highlighting the need for analysis at both taxonomic levels. The species-level analysis more closely reflects the species' ecological preference, which is strongly correlated with sediment grain size in these marine settings (Luz et al., 2012; Cabral and Loureiro, 2013; Barata, 2021). The dominance of the finer fraction is consistent with dominantly lower-energy conditions that preferentially transport juveniles from the surrounding areas. However, storm events are common in the Algarve region (Oliveira et al., 2018) and can alter this dynamic by introducing coarser materials, which correlate with changes in biogenic densities. Coarser sediments are typically characterised by higher biogenic densities (e.g.,

Martins et al., 2007). Since the PC1 of the mineralogy and sedimentology matrix correlates strongly with textural elements, it is understandable that the ostracod zone division closely follows the zone division of the mineralogy and sedimentology data (Fig. 6).

Conversely, the genus-level cluster analysis will more closely reflect the true number of ostracod valves per sample, as many juveniles cannot be identified at the species level. Thus, the cluster analysis in the **genera dataset** will more closely reflect hydrodynamic influences on valve transportation, regardless of specific ecological preferences.

For example, the genus *Sagmatocythere* is represented by two species with distinct known depth preferences. *Sagmatocythere multifora,* an Atlantic form more typical of water depths greater than 40 m (Athersuch et al., 1989), while *S. variesculpta* has no specific depth or sediment type preference (Barata, 2021). In the genus *Cytheropteron*, the common *C. ruggierii* is a Mediterranean form that prefers waters >40 m (Bonaduce et al., 1976) with no clear sediment type preference (sand (Bonaduce et al., 1976); silt (Barata, 2021)), while the common *C. dorsocostatum* does not have a specific depth preference but prefers more silty substrates (Athersuch et al., 1989; Barata, 2021); conversely, rare *C. latum* and *C. sulcatum* prefer deeper water and sandy substrates (Bonaduce et al., 1976). Likewise, *Semicytherura*, represented by 13 species, includes forms with distinct ecological preferences and geographic range. The three cited genera are also excellent examples of genera with a high percentage of juveniles identified only to the genus level, individuals not included in the species-level analysis.

5.3. Source of the sediments

Calcite is the dominant mineral in the POP14 core, with terrigenous minerals, including quartz, feldspars, and phyllosilicates (such as illite and kaolinite), as secondary constituents. The high calcite and carbonate contents in this record do not solely attest to biogenic *in situ* activity. Carbonates, Ca_{Mg}, and sand clustering opposite calcite and quartz in PC1 of the mineralogy and sedimentology matrix indicate a balance between two primary particle sources: a biogenic source and a terrigenous source (e.g., Oliveira et al., 2007).

Regarding the biogenic source, the high species richness indicates a relatively high primary productivity area, likely an effect of increased coastal upwelling conditions (Luz et al., 2012). Regarding the terrigenous source, the dominance of the finer fraction is consistent with dominantly lower-energy conditions. However, common storm-induced currents that transport sediment from other sections of the continental shelf also impact sediment deposition in this area (Feist et al., 2023). These high-energy events typically transport coarser material. Coastal and shelf deposits are primarily the result of coastal cliff erosion in this section of the Algarve (e.g., Dias et al., 2000). The coastal southwest Algarve is predominantly composed of limestones, silts, marls, beach rock, sands, and gravels (e.g., Chester, 2012).

5.4. Changes in depositional environments

Ostracod assemblages are highly influenced by sediment texture. Therefore, we follow PC1 from the mineralogical and sedimentological data to establish three primary zones (MSZ-I to III) spanning the last ca. 4000 cal yrs BP. Fig. 6 highlights the zone boundaries among the various proxies.

5.4.1. MSZ-I: ca. 2296 – ca. 3900 cal yrs BP

OZ-S1 and OZ-S2 are characterised by opposing geochemical, sedimentological conditions and species richness (Fig. 6), suggesting highly fluctuating hydrodynamic conditions in the oldest section of the core. OZ-S1 displays the highest species richness (number of species) and follows a period of reduced detrital input and an increase in mean grain size (Fig. 6). Together, these proxies suggest OZ-S1 represents a period of higher hydrodynamic activity, possibly driven by regularly occurring high-energy events. Coarser sediments, enriched in detrital minerals and carbonate particles, and often characterised by increased biogenic density, are typically associated with higher intensities of bottom currents (e.g., Martins et al., 2007). Interestingly, Mendes et al. (2020) also observed bivalve shells enrichment in a marine core collected close to V. R. S. António (Fig. 1) at certain levels around 3600 cal yr BP; the authors considered that this enrichment may result from episodes of storm wave winnowing and subsequent redistribution and deposition of high-energy event sediments.

In contrast, OZ-S2 follows a period of slight increase in Al/Ca and Si/Ca and is predominantly fine-grained (~66 %). This zone also lacks several deeper-water ostracod species and the two non-phytal littoral scarce species (Figs. 4 and 6), suggesting OZ-S2 is characterised by generally lower-energy depositional conditions, hindering transport of ostracod valves from adjacent areas.

The impact of tsunamis, which can disturb ostracod valve accumulation, was also considered when assessing the OZ-S1 – OZ-S2 transition. However, we detected no signs of sedimentary hiatuses that are expected to occur in response to high-energy events such as tsunamis (e.g., Schneider et al., 2010; Trog et al., 2015). Moreover, no indications of increased terrestrial input were observed (e.g., Kümmerer et al., 2020). Therefore, although Feist et al. (2023) documented a tsunami event in the western Algarve around 3600 cal yrs BP, our data show no evidence of such a disturbance in our site, at 85 m depth.

Throughout OZ-S3, sediments are predominantly fine-grained (>60 %) and are periodically intercalated with coarse material. The reduced variability of detrital elements suggests a relatively constant input of sediments to the shelf (e.g., Kümmerer et al., 2020), with homogeneous background conditions regularly disturbed by higher-energy episodes (e.g., Val-Peón et al., 2021). Still, OZ-S3b exhibits lower mean grain size variation compared to OZ-S3a, with a rebound in species richness comparable to that of OZ-S1 occurring in OZ-S3b only (Fig. 6). Taken together, the proxies suggest that hydrodynamic conditions favourable to the accumulation of ostracod valves gradually improved through OZ-S3.

MSZ-I, as defined in this study, corresponds to a period with few published paleorecords in Algarve (specifically, from 6000 to 2000 cal yrs BP; Mendes et al., 2020). The existing paleorecords indicate a warm and dry climate after 5000 cal yrs BP, interrupted by periodic extreme arid events (Fletcher et al., 2007) or short-lived precipitation events until 1500–1200 cal yrs BP (Mendes et al., 2010, 2020). Mendes et al. (2020), nevertheless, stress that from ca. 5800 to ca. 1300–1200 cal yr BP the depositional conditions were characterised by a paucity of flooding events, reflecting marine winnowing of bypassed material and local erosional processes, conditioned by low river discharges and/or high-energy waves. This aligns with the general trend of decreasing terrestrial input (Al/Ca and Si/Ca) observed in our core throughout ostracod OZ-S2 and OZ-S3, which extends into MSZ-II until ~45 cm (1292 (1092–1494) cal yrs BP) of water depth (Fig. 6).

Similar interpretations are proposed in other paleorecords from southwestern Iberia. Ortega and Garzón (2009) describe the Guadiana River basin in southwestern Spain as being under a predominantly dry phase, interrupted by rare flooding events. Benito et al. (2015) review study of floods in the Iberian Peninsula further supports this interpretation. However, the authors emphasise that regional precipitation variability was likely, as confirmed by subsequent studies in Iberia; for instance, in the Tagus prodelta (offshore Lisbon), periodic high discharges were recorded between ca. 5750–2200 cal yrs BP (Dessandier et al., 2018); in contrast, in the Sado estuary further south, significant changes in the precipitation regime were more restricted, particularly between ca. 3570 and 3240 cal. BP (Costa et al., 2019).

5.4.2. MSZ-II: ca. 853 – ca. 2296 cal yrs BP

MSZ-II continues showing cyclic variations in Al/Ca and Si/Ca, though within the general trend of decrease in terrestrial inputs, reversed by increases in biogenic proxies (Ca) and primary productivity (Br) until ~45 cm (1292 cal yrs BP (1092–1494)). At this point,

terrestrial input rises (Fig. 6), accompanied by a rise in land moisture (Fe, Mn). Together, these results suggest a transitional phase, likely driven by increased precipitation in the region (e.g., Mendes et al., 2020).

However, when comparing our geochemical data with the sedimentological data, the increase in fine-sediment fraction does not occur until ~30 cm depth (853 (684–1008) cal yrs BP; Fig. 6). Even considering differences in sampling resolution, this suggests a lag in sedimentary response to hydrological shifts, possibly due to threshold conditions for grain size changes or differential mineral transport.

The CONISS analysis at both taxonomic levels supports the temporal mismatch. The genus-level analysis aligns with the geochemical signal, suggesting that hydrodynamic conditions changed in the area after ~45 cm, which affected ostracod accumulation. Conversely, the species-level analysis tracks the mean grain size data, which only begins to change at ~30 cm depth (Fig. 6).

These observations suggest that changes in hydrodynamics do not always translate into changes in mean grain size. A slight increase in secondary minerals, such as plagioclase and feldspar, after ca. 1292 (1092–1494) cal yrs BP (Fig. 6), supports a scenario of enhanced cliff erosion and terrestrial input, potentiated by increased precipitation and/or coastal drift. The sediment maturity relationship (quartz/[feldspar + plagioclase]) supports this interpretation (Fig. 6). However, because feldspars and illite are relatively sensitive to weathering (e.g., Oliveira et al., 2007), their enrichment implies a more localised origin. Consequently, the fine-to-coarse mineral ratio (illite/[quartz + feldspar + plagioclase]) provides insight into hydrodynamic activity that may not be inferred from the grain size data alone.

The pattern observed in POP14 aligns with other studies from the Algarve, showing a transition from arid to wetter conditions, with the timing of this shift varying between 1500 and 1000 cal yrs BP, depending on the study (e.g., Mendes et al., 2010, 2020; Rosa et al., 2011). In sediment cores collected in the vicinity of the Guadiana River mouth (V. R. S. António, Fig. 1), this climatic transition is characterised by an increase in fine particle deposition of fluvial origin. A record from central Algarve (Faro, Fig. 1), however, shows weaker river input (Abrantes et al., 2017), despite a more pronounced fluvial influence in this part of the Algarve than in our study area.

Positive-to-neutral NAO conditions persisted for most of the middle to late Holocene (Olsen et al., 2012). However, there were also periods of transitions to neutral or negative NAO indices during this period (Olsen et al., 2012). Moreover, the climate variability in the Iberian Peninsula at centennial-scale intervals does not reflect solely the prevailing NAO phases and the clustering of extreme NAO episodes. Other modes, such as the East Atlantic (EA) and Scandinavian (SCA) patterns, also modulate the climate in Iberia (Abrantes et al., 2017; Moreno et al., 2019), affecting regional precipitation variability (e.g., Abrantes et al., 2017). This climate variability involved complex spatial gradients across the Iberian Peninsula (Lebreiro et al., 2006; Sánchez-López et al., 2016) during the MSZ-II time frame, as defined here.

The Roman Period (RP) is broadly associated with a dominant negative NAO and warm conditions (Abrantes et al., 2017). Records in the Algarve point to overall dry conditions (e.g., Fletcher et al., 2007; Mendes et al., 2020). On the other hand, the Atlantic W Portuguese Margin was characterised by intensified rainfall (e.g., Lebreiro et al., 2006; Dessandier et al., 2018). In the Iberian central range (central Spain), however, early RP was highly variable, characterised by alternating cold and warm periods, as evidenced by short-term fluctuations in intense runoff and soil erosion in an alpine lacustrine record (Sánchez-López et al., 2016). Conversely, marine cores from the Mediterranean (Algerian-Balearic basin) showed an increase in fluvial input during the latter part of the RP (Moreno et al., 2012).

The subsequent period, the Early Middle Ages interval (EMA; 500–900 CE; 1450–1050 cal yrs BP), was also characterised by contrasting biogeographic conditions: generally humid in northeastern Iberia, arid-to-humid in central Iberia, and the south remained dry (Sánchez-López et al., 2016).

Persistent positive NAO conditions returned in the subsequent Medieval Climate Anomaly (MCA; 900–1300 CE; 1050–650 cal yr BP; Olsen et al., 2012; Trouet et al., 2009). This typically leads to drier conditions across northwestern Africa, Iberia, and south-central Europe (Moreno et al., 2012; Sánchez-López et al., 2016). However, studies reveal that the MCA climatic anomaly was also characterised by complex biogeographic-climatic variation across Iberia (Abrantes et al., 2017), even at short distances. A review of marine and terrestrial records for Iberia by Moreno et al. (2012) identifies increased humidity in northwestern Iberia, contrasting with the warm, drier conditions in southern Iberia. Abrantes et al. (2017) identified two distinct phases in the MCA in northwestern Iberia: an early period was characterised by intense precipitation and flooding, warm winters, and a cooler spring–fall season, while the late MCA had relatively drier, cooler winters and a warmer spring–fall season. Conversely, in central Algarve, drier conditions persisted throughout the MCA, with a slight decrease in the fine sediment fraction observed (Abrantes et al., 2017; Mil-Homens et al., 2017). Records from the Guadiana River mouth, on the other hand, show little to no decrease in terrigenous input of fluvial origin during the MCA (Mendes et al., 2010, 2020; Rosa et al., 2011), reflecting regional geomorphological differences and the influence of river discharge. The Guadiana River is the primary fluvial influence in the Algarve (Mendes et al., 2010; Mil-Homens et al., 2017).

5.4.3. MSZ-III: ca. 91 – ca. 853 cal yrs BP

MSZ-III is characterised by a shift in PC1 sedimentology and mineralogy values (more negative values), reflecting an increase in the fine sediment fraction (Fig. 3A and 6), accompanied by continued generally elevated concentrations of terrigenous elements (e.g., Al). Our ostracod data also suggest changes in hydrodynamic conditions that were less favourable for the accumulation of ostracod valves. This is reflected in reduced absolute abundances and a decline in species richness within OZ-S5 (Fig. 6).

MSZ-III, as defined in our study, encompasses the transition from MCA overall NAO index-positive conditions to the negative NAO conditions associated with the Little Ice Age (LIA; 1300–1850 CE; 650–100 years BP; Olsen et al., 2012). While the MCA was generally warm across Iberia, characterised by biogeographical variation in precipitation, LIA, in contrast, was a period during which wet and cold conditions largely prevailed across the Iberian Peninsula (Sánchez-López et al., 2016).

In Algarve, the colder and wetter conditions associated with the LIA are reflected in increased fluvial input (Abrantes et al., 2017; Mil-Homens et al., 2017) and a depositional regime dominated by fine-grained fluvial sediments (Mendes et al., 2010, 2020; Rosa et al., 2011). This generally aligns with our results, showing continued high terrestrial input and an increase in the percentage of finer sediment compared to the MCA period. Overall, reductions in coastal upwelling conditions have been reported in the literature (e.g., Dessandier et al., 2018), confirming the changes in hydrodynamics suggested by our ostracod data; nevertheless, periodic, intense upwelling conditions were also noted during this period, demonstrating that the LIA was environmentally unstable (Dessandier et al., 2018).

In west-central Portugal (Buraca Gloriosa cave), LIA was identified as the most enduring wet interval in a detrended isotopic record dating back to 9000 cal yrs BP (Thatcher et al., 2020). Studies across Iberia confirm this pattern, suggesting predominantly wet conditions, high frequency of storms, and episodic paleo-floods (e.g. Moreno et al., 2019; Sánchez-López et al., 2016). On the other hand, records of arboreal pollen (indicative of a reduction in forest cover across Portugal) and regional sea surface temperature studies (alkenone-based SST), corroborate the colder conditions of the LIA, contrasting with MCA's overall warmer conditions (e.g., Abrantes et al., 2017 and references therein).

The more recent shift to warmer and drier conditions (after ca. 50 cal yrs BP), associated with a return to positive NAO phases and an increase in EA mode, falls outside the temporal range of our record (Abrantes

et al., 2017; Moreno et al., 2019; Santos et al., 2024).

5.5. Anthropogenic signal in POP14

Soil degradation, linked to intensified deforestation and land-use practices during the RP and MCA, is not reflected in our record through significant changes in the sedimentation rates. This absence is expected, given the limited run-off sediment from the region's small tributaries (Lobo et al., 2004; Feist et al., 2023). This data agrees with records from central Algarve (Mil-Homens et al., 2016).

The onset of wetter conditions between 1500 and 1000 cal yrs BP (Mendes et al., 2010, 2020; Rosa et al., 2011) and during the LIA favoured the deposition of fine-grained particles on the shelf near the Guadiana River (Mendes et al., 2010: 2020; Rosa et al., 2011) and in central Algarve (Mil-Homens et al., 2016, 2017; Abrantes et al., 2017). In our record, the geochemical data reflect the climatic transition, whereas changes in mean grain size show a more gradual fining trend. The intensification of human activities during this time probably further favoured the supply of fine-grained terrestrial sediments to the shelf (Burdloff et al., 2008).

In POP14, prominent signals of human activities are seen in distinct Pb concentration peaks at 47 cm (1448 (1142–1552) cal yrs BP) and ~70–65 cm. The peak at 47 cm of depth coincides with the onset of the EMA, a wetter phase that would enhance element transport to the continental shelf. Conversely, the highest Pb concentration at ca. 1893 (1632–2137) cal yrs BP, and the peak at ca. 2009 (1736–2260) cal yrs BP, coincide with the RP (−200–500 CE; 1450–2150 cal yrs BP), a period known for extensive agricultural expansion (Fletcher et al., 2007) and mining activities associated with the Iberian Pyrite Belt, as also confirmed from other studies on Pb concentration variation in the Algarve (e.g., Delgado et al., 2012; Mil-Homens et al., 2016, 2017). The increase in Pb concentration in the upper 15 cm of our core likely reflects intensified anthropogenic influence during the 19th-century Industrial Revolution, consistent with regional records (Mil-Homens et al., 2016).

6. Conclusion

- *Costa runcinata* is the only dominant, ostracod autochthonous species.
- POP14 high species richness and evenness reflect the combined influence of the dominant easterly superficial flow of the NASW, the wind-induced upwelling between March and September, and the S-SW counter-current of Mediterranean origin along the Algarve coast. Moreover, the bathymetric location of the study site promotes the accumulation of valves.
- The species-level analysis reflects changes in sedimentary texture, while the genus-level analysis captures broader hydrodynamic patterns due to higher juvenile representation.
- PC1 Geochemical analysis signals a climatic transition at ~45 cm (~1292 (1092–1494) cal yrs BP), reflecting increased terrestrial/detrital input (Al, Si). Prior to this shift, conditions were relatively homogenous, regularly disturbed by higher-energy episodes.
- The ostracod data reveal finer-scale hydrodynamic variability and offer greater sensitivity to oceanographic conditions than sedimentological or geochemical proxies.
- Evidence from multiple western Algarve settings indicates the region's susceptibility to extreme wave events during this period. However, the resolution of our dataset limits the interpretation of their impact on the ostracod data accumulation patterns.
- Anthropogenic activity is detected in Pb concentration peaks, with the highest concentration occurring during the Roman Period.

CRediT authorship contribution statement

Maria João Fernandes Martins: Writing – review & editing, Writing – original draft, Visualization, Validation, Resources, Methodology, Investigation, Formal analysis, Data curation. **Maria Cristina Cabral:** Writing – review & editing, Validation, Resources, Methodology, Investigation, Data curation. **Vitor Hugo Magalhães:** Writing – review & editing, Validation, Methodology, Investigation, Data curation. **Teresa Drago:** Writing – review & editing, Validation, Resources, Project administration, Methodology, Investigation, Funding acquisition, Data curation, Conceptualization. **Francisco Fatela:** Writing – review & editing, Methodology, Investigation. **Anabela Oliveira:** Writing – review & editing, Investigation, Data curation.

Declaration of competing interest

The authors declare that they have no known competing financial interests or personal relationships that could have appeared to influence the work reported in this paper.

Acknowledgements

We thank Isabel Mendes for a helpful discussion of an earlier version of this manuscript and the two anonymous reviewers for their insightful comments, which improved this article. This work was supported by the Portuguese Science Foundation (FCT) I.P./MCTES through national funds (PIDDAC) -UID/50019/2025 (https://doi.org/10.54499/UIDB/50019/2020) and LA/P/0068/2020 (https://doi.org/10.54499/LA/P/0068/2020). This work also received support from the FCT under grant number 2021.01680.CEECIND, and projects UIDP/04211/2020-IHC-PROGRAMÁTICO, UIDB/04211/2020-IHC-BASE, and PDCT/MAR/55618/2004.

Appendix A. Supplementary data

Supplementary data to this article can be found online at https://doi.org/10.1016/j.quaint.2025.110114.

Data availability

All data supporting the findings of this study are available within the paper or as supplementary data.

References

Abrantes, F., Rodrigues, T., Rufino, M., Salgueiro, E., Oliveira, D., Gomes, S., Oliveira, P., Costa, A., Mil-Homens, M., Drago, T., Naughton, F., 2017. The climate of the common era off the Iberian peninsula. Clim. Past 13, 1901–1918. https://doi.org/10.5194/cp-13-1901-2017.

Andrade, C., Contente, J., Santos, J.A., 2021. Climate change projections of aridity conditions in the Iberian Peninsula. Water (Switzerland) 13. https://doi.org/10.3390/w13152035.

Aquino-López, M.A., Blaauw, M., Christen, J.A., Sanderson, N.K., 2018. Bayesian analysis of 210 Pb dating. J. Agric. Biol. Environ. Stat. 23, 317–333. https://doi.org/10.1007/s13253-018-0328-7.

Athersuch, J., Horne, D.J., Whittaker, J.E., 1989. Marine and brackish water ostracods (superfamilies Cypridacea and Cytheracea): keys and notes for the identification of the species. In: Linnean Society of London and the Estuarine and brackish-water Sciences Association. Brill EJ, Leiden.

Avolio, M.L., Forrestel, E.J., Chang, C.C., Pierre, K.J. La, Burghardt, K.T., Smith, M.D., 2019. Demystifying dominant species. New Phytol. 223, 1106–1126. https://doi.org/10.1111/nph.15789.

Báez, J.C., Gimeno, L., Real, R., 2021. North Atlantic oscillation and fisheries management during global climate change. Rev. Fish Biol. Fish. 31, 319–336. https://doi.org/10.1007/s11160-021-09645-z.

Barata, F.P.P., 2021. Associações actuais de Ostracodos da plataforma continental este algarvia, Portugal (Masters in Geologia). Faculdade de Ciências da Universidade de Lisboa, Lisboa. https://repositorio.ul.pt/handle/10451/48168.

Benito, G., Macklin, M.G., Zielhofer, C., Jones, A.F., Machado, M.J., 2015. Holocene flooding and climate change in the mediterranean. Catena 130, 13–33. https://doi.org/10.1016/j.catena.2014.11.014.

Bicho, N.F., 2009. On the edge: early Holocene adaptations in Southwestern Iberia. J. Anthropol. Res. 65, 185–206. https://doi.org/10.3998/jar.0521004.0065.202.

Blaauw, M., Christen, J.A., 2011. Flexible paleoclimate age-depth models using an autoregressive gamma process. Bayesian Anal. 6, 457–474. https://doi.org/10.1214/11-BA618.

Bonaduce, G., Ciampo, G., Masoli, M., 1976. Ostracods as Ecological and Palaeoecological Indicators. Publicazioni della Stazione Zoologica di Napoli.
Boski, T., Moura, D., Veiga-Pires, C., Camacho, S., Duarte, D., Scott, D.B., Fernandes, S. G., 2002. Postglacial sea-level rise and sedimentary response in the Guadiana Estuary, Portugal/Spain border. Sediment. Geol. 150, 103–122. https://doi.org/10.1016/S0037-0738(01)00270-6.
Burdloff, D., Araújo, M.F., Jouanneau, J.M., Mendes, I., Monge Soares, A.M., Dias, J.M. A., 2008. Sources of organic carbon in the Portuguese continental shelf sediments during the Holocene period. Appl. Geochem. 23, 2857–2870. https://doi.org/10.1016/j.apgeochem.2008.04.018.
Cabral, M.C., Loureiro, I.M., 2013. Overview of recent and Holocene ostracods (Crustacea) from brackish and marine environments of Portugal. J. Micropalaeontol. 32, 135–159. https://doi.org/10.1144/jmpaleo2012-019.
Cabral, M.C., Luz, C., Fatela, F., 2011. First survey of recent ostracods from the continental shelf of Western Algarve, South Portugal. Joannea - Geol. Paläontol. 11, 39–41.
Camacho, S., Boski, T., Moura, D., Scott, D., Connor, S., Pereira, L., 2017. Paleoenvironmental evolution of the Guadiana Estuary, Portugal, during the Holocene: a modern Foraminifera analog approach. Holocene 27, 197–235. https://doi.org/10.1177/0959683616658526.
Cardoso, J.L., 2002. Pré-História De Portugal. Editorial Verbo, Lisboa.
Chester, D.K., 2012. Pleistocene and Holocene geomorphological development in the Algarve, southern Portugal. Geomorphology 153–154, 17–28. https://doi.org/10.1016/j.geomorph.2012.01.020.
Costa, A.M., Freitas, M.D.C., Leira, M., Costas, S., Costa, P.J., Andrade, C., Bao, R., Duarte, J., Rodrigues, A., Cachão, M., Araújo, A.C., Diniz, M., Arias, P., 2019. The role of climate, marine influence and sedimentation rates in late-holocene estuarine evolution (SW Portugal). Holocene 29, 622–632. https://doi.org/10.1177/0959683618824768.
Costa, M., Silva, R., Vitorino, J., 2001. Contribuição para o estudo do clima e agitação marinha na costa Portuguesa. In: 2ª Jornadas Portuguesas De Engenharia Costeira E Portuária. Associação Nacional De Navegação. Sines.
Craft, C.B., Seneca, E.D., Broome, S.W., 1991. Loss on ignition and kjeldahl digestion for estimating organic carbon and total nitrogen in Estuarine Marsh soils: calibration with dry combustion. Estuaries 14, 175–179.
Delgado, J., Boski, T., Nieto, J.M., Pereira, L., Moura, D., Gomes, A., Sousa, C., García-Tenorio, R., 2012. Sea-level rise and anthropogenic activities recorded in the late Pleistocene/Holocene sedimentary infill of the Guadiana Estuary (SW Iberia). Quat. Sci. Rev. 33, 121–141. https://doi.org/10.1016/j.quascirev.2011.12.002.
Dessandier, P.-A., Bonnin, J., Malaizé, B., Lambert, C., Tjallingii, R., Warden, L., Sinninghe Damsté, J.S., Kim, J.-H., 2018. Variations in benthic foraminiferal assemblages in the Tagus mud belt during the last 5700 years: implications for Tagus River discharge. Palaeogeogr. Palaeoclimatol. Palaeoecol. 496, 225–237. https://doi.org/10.1016/j.palaeo.2018.01.040.
Dias, J.M.A., Boski, T., Rodrigues, A., Magalhães, F., 2000. Coastline evolution in Portugal since the last Glacial Maximum until present - a synthesis. Mar. Geol. 170, 177–186. https://doi.org/10.1016/S0025-3227(00)00073-6.
Ejarque, A., Julià, R., Reed, J.M., Mesquita-Joanes, F., Barba, J.M., Riera, S., 2016. Coastal evolution in a mediterranean microtidal zone: mid to late holocene natural dynamics and human management of the castelló lagoon, NE Spain. PLoS One 11. https://doi.org/10.1371/journal.pone.0155446.
Feist, L., Costa, P.J.M., Bellanova, P., Bosnic, I., Santisteban, J.I., Andrade, C., Brückner, H., Duarte, J.F., Kuhlmann, J., Schwarzbauer, J., Vött, A., Reicherter, K., 2023. Holocene offshore tsunami archive – tsunami deposits on the Algarve shelf (Portugal). Sediment. Geol. 448, 106369. https://doi.org/10.1016/j.sedgeo.2023.106369.
Feist, L., Costa, P.J.M., Santisteban, J.I., Albers, S., Bellanova, P., Bosnic, I., Batist, M. De, Duarte, J.F., Rodrigues, A., Reicherter, K., 2025. Shallow seismic stratigraphy of the southwestern Algarve shelf (Portugal) and characteristics of offshore tsunami deposits. Mar. Geol. 480, 107463. https://doi.org/10.1016/j.margeo.2024.107463.
Fiúza, A.F. de G., Macedo, M.E. de, Guerreiro, M.R., 1982. Climatological space and time variation of the Portuguese coastal upwelling. Oceanol. Acta 5, 31–40.
Flemming, B.W., 2000. A revised textural classification of gravel-free muddy sediments on the basis of ternary diagrams. Cont. Shelf Res. 20 (Issues 10–11), 1125–1137. https://doi.org/10.1016/S0278-4343(00)00015-7.
Fletcher, W.J., Boski, T., Moura, D., 2007. Palynological evidence for environmental and climatic change in the lower Guadiana valley, Portugal, during the last 13000 years. Holocene 17, 481–494. https://doi.org/10.1177/0959683607077027.
Garel, E., Laiz, I., Drago, T., Relvas, P., 2016. Characterisation of coastal counter-currents on the inner shelf of the Gulf of Cadiz. J. Mar. Syst. 155, 19–34. https://doi.org/10.1016/j.jmarsys.2015.11.001.
Heaton, T.J., Köhler, P., Butzin, M., Bard, E., Reimer, R.W., Austin, W.E.N., Bronk Ramsey, C., Grootes, P.M., Hughen, K.A., Kromer, B., Reimer, P.J., Adkins, J., Burke, A., Cook, M.S., Olsen, J., Skinner, L.C., 2020. Marine20—The marine radiocarbon age calibration curve (0–55,000 cal BP). Radiocarbon 62, 779–820. https://doi.org/10.1017/RDC.2020.68.
Hernández-Molina, F.J., Fernández-Salas, L.M., Lobo, F., Somoza, L., Díaz-Del-Río, V., Dias, J.M.A., 2000. The infralittoral prograding wedge: a new large-scale progradational sedimentary body in shallow marine environments. Geo Mar. Lett. 20, 109–117. https://doi.org/10.1007/s003670000040.
Hindson, R., Andrade, C., Parish, R., 1999. A microfaunal and sedimentary record of environmental change within the late Holocene sediments of Boca do rio (Algarve, Portugal). Geol. Mijnbouw 77, 311–321.
Juggins, S., 2024. Rioja: Analysis of Quaternary Science Data.. https://cran.r-project.org/package=rioja.
Kümmerer, V., Drago, T., Veiga-Pires, C., Silva, P., Magalhães, V., Mena, A., Lopes, A., Rodrigues, A.I., Schmidt, S., Silva, P.F., Terrinha, P., Baptista, M.A., 2020. Exploring offshore sediment evidence of the 1755 CE tsunami (Faro, Portugal): implications for the study of outer shelf tsunami deposits minerals. Minerals 10, 731. https://doi.org/10.3390/min10090731ï.
Lebreiro, S.M., Francés, G., Abrantes, F.F.G., Diz, P., Bartels-Jónsdóttir, H.B., Stroynowski, Z.N., Gil, I.M., Pena, L.D., Rodrigues, T., Jones, P.D., Nombela, M.A., Alejo, I., Briffa, K.R., Harris, I., Grimalt, J.O., 2006. Climate change and coastal hydrographic response along the Atlantic Iberian margin (Tagus Prodelta and Muros Ría) during the last two millennia. Holocene 16, 1003–1015. https://doi.org/10.1177/0959683606hl990rp.
Li, C., Zwiers, F., Zhang, X., Chen, G., Lu, J., Li, G., Norris, J., Tan, Y., Sun, Y., Liu, M., 2019. Larger increases in more extreme local precipitation events as climate warms. Geophys. Res. Lett. 46, 6885–6891. https://doi.org/10.1029/2019GL082908.
Lobo, F.J., Sánchez, R., González, R., Dias, J.M.A., Hernández-Molina, F.J., Fernández-Salas, L.M., Díaz Del Río, V., Mendes, I., 2004. Contrasting styles of the Holocene highstand sedimentation and sediment dispersal systems in the northern shelf of the Gulf of Cadiz. Cont. Shelf Res. 24, 461–482. https://doi.org/10.1016/j.csr.2003.12.003.
Lopes, F., Cunha, P., 2010. A Plataforma Continental Algarvia e Provincias Adjacentes: uma Análise Geomorfológica. Ciências Geológicas: Ensino, Investigação e sua História - Geologia Clássica. Publicação Comemorativa do "Ano International do planeta terra", Associação Portuguesa de Geólogos Sociedade Geológica de Portugal I, 479–490.
Luz, C., 2011. Variações Sazonais Das Associações De Foraminíferos E Ostracodos Da Plataforma Continental Algarvia: Avaliação Da Influência Do Upwelling Costeiro (Mestrado em Geologia Do Ambiente, Riscos Geológicos E Ordenamento Do Território). Faculdade de Ciências da Universidade de Lisboa, Lisboa. http://hdl.handle.net/10451/9270.
Luz, C., Fatela, F., Cabral, M.C., Drago, T., Rodrigues, A., 2012. Variações sazonais das associações de foraminíferos e ostracodos da plataforma continental algarvia. In: 2º Jornadas De Engenharia Hidrográfica, pp. 227–230.
Martins, V., Dubert, J., Jouanneau, J.M., Weber, O., Silva, E.F. da, Patinha, C., Alveirinho Dias, J.M., Rocha, F., 2007. A multiproxy approach of the Holocene evolution of shelf-slope circulation on the NW Iberian Continental shelf. Mar. Geol. 239, 1–18. https://doi.org/10.1016/j.margeo.2006.11.001.
Mazzini, I., Aiello, G., Frenzel, P., Pint, A., 2021. Marine and marginal marine Ostracoda as proxies in geoarchaeology. Mar. Micropaleontol. 174, 102054. https://doi.org/10.1016/j.marmicro.2021.1020.
Mayewski, P.A., Rohling, E.E., Stager, J.C., Karlén, W., Maasch, K.A., Meeker, L.D., Meyerson, E.A., Gasse, F., Kreveld, S. van, Holmgren, K., Lee-Thorp, J., Rosqvist, G., Rack, F., Staubwasser, M., Schneider, R.R., Steig, E.J., 2004. Holocene climate variability. Quat. Res. 62, 243–255. https://doi.org/10.1016/j.yqres.2004.07.001.
Mendes, I., Lobo, F.J., Hanebuth, T.J.J., López-Quirós, A., Schönfeld, J., Lebreiro, S., Reguera, M.I., Antón, L., Ferreira, Ó., 2020. Temporal variability of flooding events of Guadiana River (Iberian Peninsula) during the middle to late Holocene: imprints in the shallow-marine sediment record. Palaeogeogr. Palaeoclimatol. Palaeoecol. 556, 109900. https://doi.org/10.1016/j.palaeo.2020.109900.
Mendes, I., Rosa, F., Dias, J.A., Schönfeld, J., Ferreira, Ó., Pinheiro, J., 2010. Inner shelf paleoenvironmental evolution as a function of land-ocean interactions in the vicinity of the Guadiana river, SW Iberia. Quat. Int. 221, 58–67. https://doi.org/10.1016/j.quaint.2009.10.037.
Mestdagh, T., Lobo, F.J., Llave, E., Hernández-Molina, F.J., Rooij, D. Van, 2019. Review of the late Quaternary stratigraphy of the northern Gulf of Cadiz continental margin: new insights into controlling factors and global implications. Earth Sci. Rev. 198, 102944. https://doi.org/10.1016/j.earscirev.2019.102944.
Mil-Homens, M., Vale, C., Brito, P., Naughton, F., Drago, T., Raimundo, J., Anes, B., Schmidt, S., Caetano, M., 2017. Insights of Pb isotopic signature into the historical evolution and sources of Pb contamination in a sediment core of the southwestern Iberian Atlantic shelf. Sci. Total Environ. 586, 473–484. https://doi.org/10.1016/j.scitotenv.2017.01.204.
Mil-Homens, M., Vale, C., Naughton, F., Brito, P., Drago, T., Anes, B., Raimundo, J., Schmidt, S., Caetano, M., 2016. Footprint of roman and modern mining activities in a sediment core from the southwestern Iberian Atlantic shelf. Sci. Total Environ. 571, 1211–1221. https://doi.org/10.1016/j.scitotenv.2016.07.143.
Moal-Darrigade, P., Ducassou, E., Giraudeau, J., Bahr, A., Kaboth-Bahr, S., Hanquiez, V., Perello, M.C., 2022. MOW strengthening and contourite development over two analog climate cycles (MIS 12–11 and MIS 2–1) in the Gulf of Cadíz: an impact on North Atlantic climate during deglaciation V and MIS 11? Global Planet. Change 208, 103721. https://doi.org/10.1016/j.gloplacha.2021.103721.
Moreno, A., Pérez, A., Frigola, J., Nieto-Moreno, V., Rodrigo-Gámiz, M., Martrat, B., González-Sampériz, P., Morellón, M., Martín-Puertas, C., Corella, J.P., Belmonte, Á., Sancho, C., Cacho, I., Herrera, G., Canals, M., Grimalt, J.O., Jiménez-Espejo, F., Martínez-Ruiz, F., Vegas-Vilarrúbia, T., Valero-Garcés, B.L., 2012. The Medieval climate anomaly in the iberian Peninsula reconstructed from marine and lake records. Quat. Sci. Rev. 43, 16–32. https://doi.org/10.1016/j.quascirev.2012.04.007.
Moreno, A., Valero-Garcés, B.L., González-Sampériz, P., Rico, M., 2008. Flood response to rainfall variability during the last 2000 years inferred from the Taravilla Lake record (Central Iberian Range, Spain). J. Paleolimnol. 40, 943–961. https://doi.org/10.1007/s10933-008-9209-3.
Moreno, J., Fatela, F., Leorri, E., Gonçalves, M.A., Gómez-Navarro, J.J., Araújo, M.F., Freitas, M.C., Trigo, R.M., Blake, W.H., Moreno, F., 2019. Foraminiferal evidence of major environmental changes driven by the sun-climate coupling in the western Portuguese coast (14th century to present). Estuar. Coast Shelf Sci. 218, 106–118. https://doi.org/10.1016/j.ecss.2018.11.030.

Munsell Colour, 1995. Munsell Soil Color Charts. Kollmorgen Instruments Corp., New Windsor, NY.

Oksanen, J., Simpson, G.L., Blanchet, F.G., Kindt, R., Legendre, P., Minchin, P.R., O'Hara, R.B., Solymos, P., Stevens, M.H.H., Szoecs, E., Wagner, H., Barbour, M., Bedward, M., Bolker, B., Borcard, D., Borman, T., Carvalho, G., Chirico, M., Caceres, M. De, Durand, S., Evangelista, H.B.A., FitzJohn, R., Friendly, M., Furneaux, B., Hannigan, G., Hill, M.O., Lahti, L., McGlinn, D., Ouellette, M.-H., Ribeiro Cunha, E., Smith, T., Stier, A., Braak, C.J.F.Ter, Weedon, J., 2025. Vegan: Community Ecology Package. https://doi.org/10.32614/CRAN.package.vegan.

Oliveira Júnior, L. de, Relvas, P., Garel, E., 2024. Upwelling processes variability and water circulation along the northern margin of the Gulf of Cadiz. Cont. Shelf Res. 281, 105310. https://doi.org/10.1016/j.csr.2024.105310.

Oliveira, A., Santos, A.I., Rodrigues, A., Vitorino, J., 2007. Sedimentary particle distribution and dynamics on the Nazaré canyon system and adjacent shelf (Portugal). Mar. Geol. 246, 105–122. https://doi.org/10.1016/j.margeo.2007.04.017.

Oliveira, T.C.A., Neves, M.G., Fidalgo, R., Esteves, R., 2018. Variability of wave parameters and Hmax/Hs relationship under storm conditions offshore the Portuguese continental coast. Ocean Eng. 153, 10–22. https://doi.org/10.1016/j.oceaneng.2018.01.080.

Olsen, J., Anderson, N.J., Knudsen, M.F., 2012. Variability of the North Atlantic Oscillation over the past 5,200 years. Nat. Geosci. 5, 808–812. https://doi.org/10.1038/ngeo1589.

Omira, R., Baptista, M.A., Miranda, J.M., 2011. Evaluating Tsunami impact on the Gulf of Cadiz Coast (Northeast Atlantic). Pure Appl. Geophys. 168, 1033–1043. https://doi.org/10.1007/s00024-010-0217-7.

Ortega, J.A., Garzón, G., 2009. Natural Hazards and Earth System Sciences A contribution to improved flood magnitude estimation in base of palaeoflood record and climatic implications-Guadiana River (Iberian Peninsula). Hazards Earth Syst. Sci 9, 229–239. https://doi.org/10.5194/nhess-9-229-2009.

Pérez-Díaz, S., Ruiz-Alonso, M., López-Sáez, J.A., Alday, A., Cava-Almuzara, A., 2024. Environmental dynamics of the western European Mediterranean landscape during the Pleistocene to Holocene transition. Veg. Hist. Archaeobotany 33, 323–341. https://doi.org/10.1007/s00334-023-00942-0.

Pielou, E.C., 1966. The measurement of diversity in different types of biological collections. J. Theor. Biol. 13, 131–144. https://doi.org/10.1016/0022-5193(66)90013-0.

R Core Team, 2022. R: a Language and Environment for Statistical Computing.

Relvas, P., Barton, E.D., 2002. Mesoscale patterns in the Cape São Vicente (Iberian Peninsula) upwelling region. J. Geophys. Res.: Oceans 107. https://doi.org/10.1029/2000jc000456, 28_1-28–23.

Rosa, F., Dias, J.A., Mendes, I., Ferreira, Ó., 2011. Mid to late Holocene constraints for continental shelf mud deposition in association with river input: the Guadiana Mud patch (SW Iberia). Geo Mar. Lett. 31, 109–121. https://doi.org/10.1007/s00367-010-0219-6.

RStudio Team, 2024. Rstudio: Integrated Development Environment for R.

Sánchez-López, G., Hernández, A., Pla-Rabes, S., Trigo, R.M., Toro, M., Granados, I., Sáez, A., Masqué, P., Pueyo, J.J., Rubio-Inglés, M.J., Giralt, S., 2016. Climate reconstruction for the last two millennia in central Iberia: the role of East Atlantic (EA), North Atlantic Oscillation (NAO) and their interplay over the Iberian Peninsula. Quat. Sci. Rev. 149, 135–150. https://doi.org/10.1016/j.quascirev.2016.07.021.

Sánchez-Leal, R.F., Bellanco, M.J., García-Lafuente, J., Naranjo, C., Sánchez-Garrido, J. C., 2017. The Mediterranean Overflow in the Gulf of Cadiz: a rugged journey. Prog. Oceanogr. 153, 66–84. https://doi.org/10.1016/j.pocean.2017.04.002.

Santos, R.N., Rodrigues, T., Naughton, F., Schefuß, E., Oliveira, D., Moreno, J., Raposeiro, P.M., Gil-Romera, G., Morgan, A., Leira, M., Gomes, S.D., Ladd, S.N., Trigo, R.M., Ramos, A.M., Hernández, A., 2024. Understanding the Atlantic influence on climate and vegetation dynamics in western Iberia over the last 2000 years. Quat. Sci. Rev. 337, 108796. https://doi.org/10.1016/j.quascirev.2024.108796.

Schneider, H., Höfer, D., Trog, C., Busch, S., Schneider, M., Baade, J., Daut, G., Mäusbacher, R., 2010. Holocene estuary development in the Algarve Region (Southern Portugal) - a reconstruction of sedimentological and ecological evolution. Quat. Int. 221, 141–158. https://doi.org/10.1016/j.quaint.2009.10.004.

Schneider, H., Höfer, D., Trog, C., Mäusbacher, R., 2016. Holocene landscape development along the Portuguese Algarve coast - a high resolution palynological approach. Quat. Int. 407, 47–63. https://doi.org/10.1016/j.quaint.2016.02.039.

Shannon, C.E., 1948. A mathematical theory of communication. Bell System Tech. J. 27, 379–423. https://doi.org/10.1002/j.1538-7305.1948.tb01338.x.

Soares, A.M.M., Valério, P., 2024. A conversão em datas de calendário das datas de radiocarbono de organismos marinhos colhidos na costa atlântica portuguesa a nova curva de calibração Marine20. Revista Portuguesa de Arqueologia 26–27, 73–89.

Straus, L.G., Altuna, J., Ford, D., Marambat, L., Rhine, J.S., Schawrcz, J.P., Vernet, J., Sebastian, S.S., 1992. Early farming in the Algarve (Southern Portugal): a preliminary view from two cave excavations near Faro. Trab. Antropol. Etnol. 32, 141–162.

Tatzber, M., Stemmer, M., Spiegel, H., Katzlberger, C., Haberhauer, G., Gerzabek, M.H., 2007. An alternative method to measure carbonate in soils by FT-IR spectroscopy. Environ. Chem. Lett. 5, 9–12.

Thatcher, D.L., Wanamaker, A.D., Denniston, R.F., Asmerom, Y., Polyak, V.J., Fullick, D., Ummenhofer, C.C., Gillikin, D.P., Haws, J.A., 2020. Hydroclimate variability from western Iberia (Portugal) during the Holocene: insights from a composite stalagmite isotope record. Holocene 30, 966–981. https://doi.org/10.1177/0959683620908648.

Trigo, R.M., Pozo-Vázquez, D., Osborn, T.J., Castro-Díez, Y., Gámiz-Fortis, S., Esteban-Parra, M.J., 2004. North Atlantic oscillation influence on precipitation, river flow and water resources in the Iberian Peninsula. Int. J. Climatol. 24, 925–944. https://doi.org/10.1002/joc.1048.

Trog, C., Hempel, R., Frenzel, P., Mäusbacher, R., 2015. Holocene palaeoenvironmental changes in three lagoons on the Algarve coast of Portugal. Palaeobiodivers. Palaeoenviron. 95, 203–221. https://doi.org/10.1007/s12549-015-0185-0.

Trog, C., Höfer, D., Frenzel, P., Camacho, S., Schneider, H., Mäusbacher, R., 2013. A multi-proxy reconstruction and comparison of Holocene palaeoenvironmental changes in the Alvor and Alcantarilha estuaries (southern Portugal). Rev. Micropaleontol. 56, 131–158. https://doi.org/10.1016/j.revmic.2013.10.003.

Trouet, V., Esper, J., Graham, N.E., Baker, A., Scourse, J.D., Frank, D.C., 2009. Persistent positive north Atlantic oscillation mode dominated the medieval climate anomaly. Science 324, 78–80. https://doi.org/10.1126/science.1166349.

Val-Peón, C., Santisteban, J.I., López-Sáez, J.A., Weniger, G.C., Reicherter, K., 2021. Environmental changes and cultural transitions in SW Iberia during the early-mid Holocene. Appl. Sci. 11. https://doi.org/10.3390/app11083580.

Wickham, H., 2016. ggplot2: Elegant Graphics for Data Analysis.